ChemPubSoc Europe

DOI: 10.1002/chem.201603884

CHEMISTRY
A European Journal
Minireview

NMR Spectroscopy

NMR Hyperpolarization Techniques of Gases

Danila A. Barskiy,[a] Aaron M. Coffey,[a] Panayiotis Nikolaou,[a] Dmitry M. Mikhaylov,[b] Boyd M. Goodson,[c] Rosa T. Branca,[d] George J. Lu,[e] Mikhail G. Shapiro,[e] Ville-Veikko Telkki,[f] Vladimir V. Zhivonitko,[g, h] Igor V. Koptyug,[g, h] Oleg G. Salnikov,[g, h] Kirill V. Kovtunov,[g, h] Valerii I. Bukhtiyarov,[i] Matthew S. Rosen,[j] Michael J. Barlow,[k] Shahideh Safavi,[k] Ian P. Hall,[k] Leif Schröder,[l] and Eduard Y. Chekmenev*[a, m]

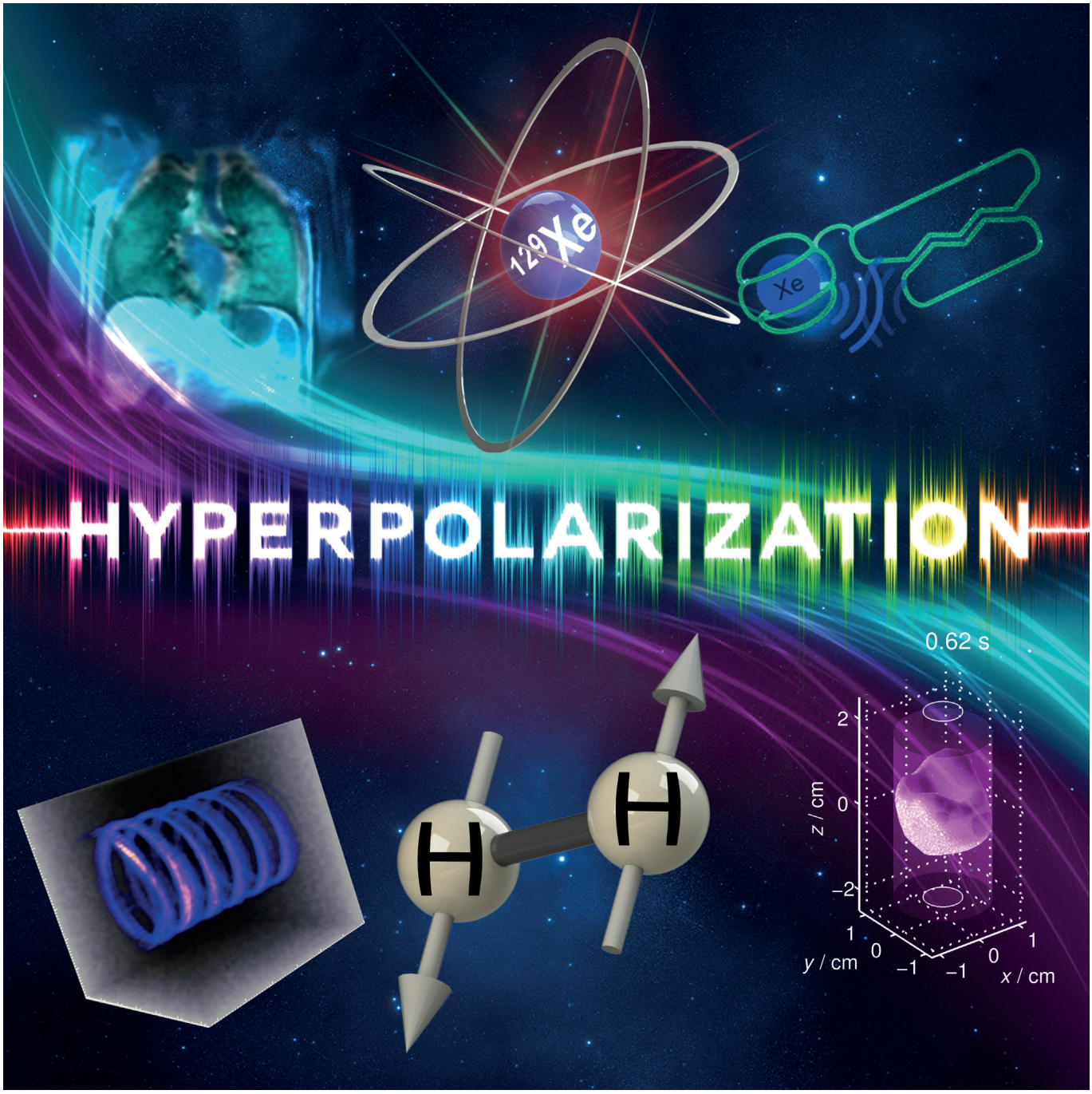

Abstract: Nuclear spin polarization can be significantly increased through the process of hyperpolarization, leading to an increase in the sensitivity of nuclear magnetic resonance (NMR) experiments by 4–8 orders of magnitude. Hyperpolarized gases, unlike liquids and solids, can often be readily separated and purified from the compounds used to mediate the hyperpolarization processes. These pure hyperpolarized gases enabled many novel MRI applications including the visualization of void spaces, imaging of lung function, and remote detection. Additionally, hyperpolarized gases can be dissolved in liquids and can be used as sensitive molecular probes and reporters. This Minireview covers the fundamentals of the preparation of hyperpolarized gases and focuses on selected applications of interest to biomedicine and materials science.

1. Introduction

The use of techniques to enhance nuclear spin polarization (*P*) to order unity (i.e., nearly 100%) results in corresponding gains in NMR sensitivity by 4–8 orders of magnitude.[1] This process of significant polarization enhancement-well above that achieved at thermal equilibrium-is termed *hyperpolarization*. Hyperpolarization of solids, liquids, and gases[2] has been demonstrated via a number of techniques including Brute Force Polarization (BFP),[3] Spin Exchange Optical Pumping (SEOP),[4] Dynamic Nuclear Polarization (DNP),[1c] Chemically-Induced Dynamic Nuclear Polarization (CIDNP)[5] photo-CIDNP,[6] Parahydrogen Induced Polarization (PHIP),[7] and Signal Amplification By Reversible Exchange (SABRE).[8] A wide range of nuclei can be hyperpolarized, including ^{1}H,[9] ^{3}He,[10] ^{7}Li,[11] ^{13}C,[1c,12] ^{15}N,[13] ^{19}F,[14] ^{31}P,[15] ^{83}Kr,[16] and ^{129}Xe,[4,17] among others.[18] Hyperpolarized (HP) substances are revolutionizing the fields of NMR spectroscopy and magnetic resonance imaging (MRI), because many applications that were previously impractical because of weak NMR signals (e.g., from sub-mM metabolites) are now becoming possible. Moreover, the enormous gain in attainable signal-to-noise ratio (SNR) allows spectroscopic detection and imaging of HP compounds to be performed in seconds, obviating the need for time-consuming signal averaging and thermal recovery of the spin magnetization. The ability to rapidly acquire signals with very high SNR from HP systems is the inherent feature that is greatly desirable for in vivo gas imaging applications: that is, images can be acquired during a single breath hold; sufficient signal can be attained despite the low density of gas compared to liquid. While liquid HP contrast agents are injected in vivo to probe metabolism[19] (extensively discussed in many recent reviews)[20] or used otherwise,[21] they typically cannot be used to probe gas-phase processes in vitro or in vivo. This Minireview focuses on the techniques allowing the production of HP gases with particular application to their use in biomedical applications, and explores some examples from materials science.

We begin with the fundamentals of SEOP in the context of NMR hyperpolarization of ^{129}Xe gas. Although other noble gases have been hyperpolarized, none are as widely used for magnetic resonance as HP ^{129}Xe, which has a relatively large natural abundance (ca. 26%) and is relatively cheap (ca. USD 20 per L). The selected applications described here include functional lung imaging,[22] metabolic brown fat imaging,[23]

[a] *Dr. D. A. Barskiy, Dr. A. M. Coffey, Dr. P. Nikolaou, Prof. E. Y. Chekmenev*
Department of Radiology, Department of Biomedical Engineering
Department of Physics, Vanderbilt-Ingram Cancer Center (VICC)
Vanderbilt University Institute of Imaging Science (VUIIS)
Vanderbilt University, Nashville, TN 37232 (USA)
E-mail: eduard.chekmenev@vanderbilt.edu

[b] *Prof. D. M. Mikhaylov*
Huazhong University of Science and Technology
Wuhan, 100044 (China)

[c] *Prof. B. M. Goodson*
Southern Illinois University
Department of Chemistry and Biochemistry, Materials Technology Center
Carbondale, IL 62901 (USA)

[d] *Prof. R. T. Branca*
Department of Physics and Astronomy
Biomedical Research Imaging Center
University of North Carolina at Chapel Hill
Chapel Hill, NC 27599 (USA)

[e] *Dr. G. J. Lu, Prof. M. G. Shapiro*
Division of Chemistry and Chemical Engineering
California Institute of Technology, Pasadena, CA 91125 (USA)

[f] *Dr. V.-V. Telkki*
NMR Research Unit, University of Oulu
90014 Oulu (Finland)

[g] *Dr. V. V. Zhivonitko, Prof. I. V. Koptyug, O. G. Salnikov, Dr. K. V. Kovtunov*
International Tomography Center SB RAS
630090 Novosibirsk (Russia)

[h] *Dr. V. V. Zhivonitko, Prof. I. V. Koptyug, O. G. Salnikov, Dr. K. V. Kovtunov*
Novosibirsk State University
Pirogova St. 2, 630090 Novosibirsk (Russia)

[i] *Prof. V. I. Bukhtiyarov*
Boreskov Institute of Catalysis SB RAS
5 Acad. Lavrentiev Pr., 630090 Novosibirsk (Russia)

[j] *Prof. M. S. Rosen*
MGH/A.A. Martinos Center for Biomedical Imaging
Boston, MA 02129 (USA)

[k] *Dr. M. J. Barlow, Dr. S. Safavi, Prof. I. P. Hall*
Respiratory Medicine Department, Queen's Medical Centre
University of Nottingham Medical School
Nottingham NG7 2UH (UK)

[l] *Dr. L. Schröder*
Molecular Imaging, Department of Structural Biology
Leibniz-Institut für Molekulare Pharmakologie (FMP)
13125 Berlin (Germany)

[m] *Prof. E. Y. Chekmenev*
Russian Academy of Sciences
119991 Moscow (Russia)

ORCID(s) from the author(s) for this article are available on the WWW under http://dx.doi.org/10.1002/chem.201603884.

Boyd M. Goodson graduated from Princeton University in 1995 (thesis research with Warren Warren and Herschel Rabitz) and earned his Ph.D. in chemistry in 1999 with Alexander Pines at the University of California, Berkeley/LBNL. Following postdoctoral work with Ahmed Zewail at Caltech, in 2002 Goodson joined the faculty at Southern Illinois University Carbondale and was promoted to full professor in 2014. His research and teaching have been recognized by an NSF CAREER award, Research Innovation and Cottrell Scholar Awards from the Research Corporation for Science Advancement, the ORAU Powe Junior Faculty Award, and the Kaplan Award for Research, Sigma Xi Society (SIUC Chapter). Goodson's research interests concern magnetic resonance and optical spectroscopies, NMR/MRI sensitivity enhancement, and hyperpolarization.

Matthew S. Rosen received his Ph.D. in Physics at the University of Michigan in 2001, where he developed the first ^{129}Xe high-volume hyperpolarizer for in vivo *use, and with it demonstrated the first use of ^{129}Xe as a MRI tracer* in vivo*. His career bridges the spectrum from fundamental physics to applied bioimaging work. He is Assistant Professor of Radiology at Harvard Medical School and the Director of the Low-Field MRI and Hyperpolarized Media Laboratory at the MGH/Martinos Center for Biomedical Imaging. He currently leads an effort to develop tools and techniques for robust ultra-low-magnetic-field implementations of MRI.*

Dr. Danila A. Barskiy studied Chemistry in Novosibirsk State University where he obtained a Ph.D. in 2015. He is currently pursuing his research interests as a Postdoctoral Fellow at the Vanderbilt University Institute of Imaging Science in the laboratory of Prof. Eduard Chekmenev. His research interests include spin dynamics and chemical kinetics of parahydrogen-based nuclear spin hyperpolarization techniques (SABRE and PHIP) and applications of these techniques for NMR spectroscopy and imaging of biomedical and industrial processes.

Prof. Dmitry Mikhaylov studied applied physics at the National Research Nuclear University MEPHI (NRNU MEPHI). He got his Ph.D. in 2011 under the guidance of Prof. M. Ivanov. In 2012 he became the head of Engineering Science Center of NRNU MEPHI, one of the biggest R&D centers in Russia. In 2012 he received one of the biggest Russian State research grants for research in the area of endoscopy. In 2013, he started collaboration with Vanderbilt University for research in field of endoscopy and nanomaterials. In 2015, he received an award from Russian Airspace Agency to conduct research in gravity free biological processes. In 2016, he moved to China to continue research.

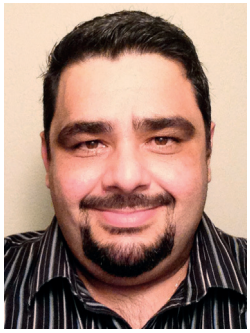

Panayiotis Nikolaou studied Chemistry with a primary focus on (i) developing and applying new technologies to understand and improve hyperpolarized ^{129}Xe production and (ii) studying the host-guest dynamics of ^{29}Xe-cryptophane inclusion complexes at Southern Illinois University Carbondale (under the guidance of Prof. Boyd M. Goodson), where he earned his Ph.D. in 2010. He is currently a Post-Doctoral fellow with Prof. Eduard Chekmenev at Vanderbilt, where he has designed and built two automated clinical-scale xenon polarizers. Current Research interests include the development of fully-automated xenon hyperpolarizer technology, hyperpolarized contrast agents, and their biomedical application in MR.

Eduard Y. Chekmenev, b 1977, Ph.D. in Physical Chemistry (supervisor Prof. Richard J. Wittebort) 2003, University of Louisville, KY, USA. Postdoctoral Fellow at NHMFL to work on structural biology of membrane proteins in Tallahassee, FL, USA (with Prof. Timothy Cross) and in NMR hyperpolarization at Caltech (with Prof. Daniel P. Weitekamp) and hyperpolarized in vivo *imaging at HMRI (with Dr. Brian D. Ross). In 2009, Dr. Chekmenev started his hyperpolarization program at Vanderbilt University Institute of Imaging Science (VUIIS), and he was tenured in 2015. In 2016, he was elected as a Professor of the Russian Academy of Sciences. Research interests include development of methods of hyperpolarization and their Biomedical and industrial applications.*

Shahideh Safavi studied Medicine at St George's University of London, graduating in 2008. She undertook her general medicine training in London, followed by specialist training in respiratory medicine in London and Nottingham. She is currently pursuing her research interests at University of Nottingham, as a clinical research fellow, under the supervision of Prof. Ian Hall and Dr. Michael Barlow. Her research is focused on development and use of novel functional MRI techniques in respiratory medicine.

Michael Barlow studied Physics at Essex University where he obtained his Ph.D. in the study of hot electron transport in semiconductor quantum wells. His interest in optical pumping arose from work on helium magnetometers when he was instrument manager for the NASA Cassini MAG team. This work continues to the present day with optical pumping and Raman techniques to explore spin exchange optical pumping for the production of hyperpolarized xenon. He is currently lead physicist for the Nottingham xenon Lung imaging team.

Professor Ian Hall is currently the Boots' Professor of Therapeutics and Director of the Centre for Biomolecular Sciences at the University of Nottingham. His main clinical interest is in respiratory medicine. He completed his clinical studies at the University of Oxford before moving to Nottingham for specialist and research training. Subsequently he was an MRC travelling fellow at the University of Pennsylvania and National Asthma Campaign Senior Research Fellow back in Nottingham. Current research interests include the genetic basis of lung disease and novel imaging approaches.

Rosa Tamara Branca studied Physics at the University of Rome La Sapienza, where she obtained her Bachelors of Science and Masters degree in 2002. In 2006 she obtained her Ph.D. in Biophysics under the guidance of Dr. B. Maraviglia and Dr. W. Warren while studying non-linear MR effects due to dipolar-dipolar interactions and radiation damping. In 2006 she moved to Duke University, first as a Post-Doctoral Fellow and then as an Assistant Research Professor (2009). She began working with hyperpolarized gases in 2009, while working on a project to detect targeted lung metastases with HP Helium. In 2012 she moved to the University of North Carolina at Chapel Hill, where she holds a faculty appointment in the Department of Physics and Astronomy and in the Biomedical Research Imaging Center. Her current research interests include applications of hyperpolarized gases in lung and brown fat imaging.

Leif Schröder studied Physics in Göttingen and Heidelberg where he obtained a Ph.D. in Physics while being affiliated with the German Cancer Research Center to investigate the quantum mechanical fine structure of in vivo NMR spectra. His subsequent stay at the University of California at Berkeley and Lawrence Berkeley National Laboratory was supported by an Emmy Noether fellowship from the German Research Foundation to work hyperpolarized xenon biosensors. He is a co-developer of the Hyper-CEST technique for which he received national and international prizes, including the IUPAP Young Scientist Award in Medical Physics. He further received an Emmy Noether fellowship to start his own group at the FMP, Berlin, where he also managed the ERC Project BiosensorImaging and is currently heading the Molecular Imaging Group.

Mikhail G. Shapiro is an Assistant Professor of Chemical Engineering and a Heritage Principal Investigator at the California Institute of Technology. His laboratory works on biomolecular technologies for non-invasive imaging and control of biological function. He received his Ph.D. in Biological Engineering from MIT and held post-doctoral fellowships at the University of Chicago and the University of California, Berkeley. He has pioneered protein-based MRI sensors of neurotransmission, reporter genes for several forms of MRI, including xenon and diffusion, and genetically encoded reporters for ultrasound. His awards include the Burroughs Wellcome Career Award, the DARPA Young Faculty Award, the Pew Biomedical Scholarship and the Technology Review's TR35 list of the top innovators under age 35.

Dr. George J. Lu obtained his B.S. degree at University of Alberta, Canada, where he worked with Prof. Brian Sykes and Prof. Michael James on protein NMR and X-ray crystallography. He received his Ph.D. at the University of California, San Diego (UCSD), where he studied solid-state NMR methodology and membrane protein structural biology with Prof. Stanley Opella. He is currently a postdoctoral fellow at Caltech with Prof. Mikhail Shapiro, and his research applies the technique of protein engineering to the development of MRI contrast agents and new imaging and therapeutic methods.

Dr. Aaron M. Coffey conducted undergraduate studies in Electrical Engineering at the University of Arizona, Tucson. He completed a Ph.D. in Biomedical Engineering in 2014 at Vanderbilt University under the guidance of Prof. Eduard Chekmenev in the area of hyperpolarized and low-field NMR and MRI, where he continued as a postdoctoral fellow. He recently received the Ruth L. Kirschstein postdoctoral fellowship 1F32EB021840-01 for 'Ultra-fast molecular MRI of human adipose tissue with hyperpolarized xenon-129 contrast agent." His research interests include advancing MR detection hardware and utilizing hyperpolarization techniques to enable MR contrast agents for molecular imaging and high sensitivity spectroscopic NMR studies.

Prof. Igor V. Koptyug received his Ph.D. degree in 1991; in 1992–1995 he was a postdoctoral researcher in the photochemistry group of Professor N. J. Turro (Columbia University, New York). He earned his Dr. Sci. (Habilitation) degree in catalysis in 2003 and a title of Professor in 2006; currently, he is the head of the Laboratory of Magnetic Resonance Microimaging at the International Tomography Center, Siberian Branch of the Russian Academy of Sciences, Novosibirsk. His research interests include signal enhancement in NMR and applications of NMR and MRI in catalysis and biological studies in vivo *and* in vitro.

Dr. Kirill V. Kovtunov studied chemistry at the Novosibirsk State University, Russia. He completed a Ph.D. in Physical Chemistry in 2008 at the International Tomography Center under the supervision of Prof. Igor Koptyug in the area of utilization of parahydrogen in heterogeneous processes, where he obtained heterogeneous PHIP effects for the first time. His research interests include heterogeneous catalysis and utilization of parahydrogen-induced polarization techniques to produce highly polarized contrast agents for NMR/MRI and mechanistic studies of heterogeneous reactions involving hydrogen. Currently, he is a senior scientific researcher in the group of Prof. Igor Koptyug.

Valerii I. Bukhtiyarov received his Ph.D. degree in 1989. In 1993, Valeriy I. Bukhtiyarov held a post-doc position at University of Wales College of Cardiff (UK) supervised by Professor M. Wyn Roberts. He earned his Dr. Sci. (Habilitation) degree in catalysis in 1998 and a title of Professor in 2003. Since 2000, he is the head of the Surface Science Laboratory in the Boreskov Institute of Catalysis (BIC) of the Siberian Branch of the Russian Academy of Sciences, Novosibirsk; since July 2015, he is the director of BIC. His scientific interests include bridging between surface science and heterogeneous catalysis; application of physical methods to study adsorption and surface chemical reactions, including in situ *measurements; and application of nanoscience approaches for modeling and study of heterogeneous catalysts.*

Oleg G. Salnikov completed his undergraduate studies in chemistry at Novosibirsk State University in 2014 and continued there as a Ph.D. student. In 2012, he started working on the HET-PHIP project in the group of Prof. Igor Koptyug at the International Tomography Center SB RAS under the supervision of Dr. Kirill Kovtunov. His research interests include the application of PHIP for mechanistic studies of heterogeneous catalytic reactions and development of MR contrast agents using HET-PHIP.

Ville-Veikko Telkki studied physics at the University of Oulu, Finland. He completed his Ph.D. studies in 2006 under the guidance of Prof. Jukka Jokisaari. In 2005, before the final dissertation, he joined the research group of Prof. Alex Pines in UC Berkeley, concentrating on remote detection MRI. In 2007, he returned back to University of Oulu. Currently, he is a Research Fellow of Academy of Finland, and he is leading the Experimental NMR Research Group, focusing on the development and application of advanced NMR methods for materials research.

Dr. Vladimir V. Zhivonitko graduated from Novosibirsk State University, Russia, in 2005, where he studied chemistry. In the same year he started his Ph.D. studies under supervision of Prof. Igor V. Koptyug at the International Tomography Center SB RAS. In 2008 he defended his Ph.D. thesis concerning MRI of nonlinear chemical processes in model catalytic reactors. Thereafter, he joined the HET-PHIP project conducted in Prof. Koptyug's lab as a postdoctoral researcher. His interests include basic NMR research with hyperpolarized substances, development of catalytic systems for PHIP and NMR micro-imaging of catalytic reactors. Currently, he works as a senior scientific researcher at the same location.

and biosensors[24] (including those enabled by genetic encoding).[25] A recent demonstration of the DNP process to hyperpolarize ^{129}Xe[26] and hydrocarbon gases[27] is also described.

HP gases can also be efficiently produced via PHIP, when parahydrogen gas is added in a pairwise manner to a multiple chemical bond (C=C or C≡C) in an unsaturated molecule, resulting in a gaseous HP product. This process can be performed in heterogeneous fashion,[9a,28] and despite low T_1 of the HP states, this powerful scalable technique allows for cheap preparation of HP hydrocarbons on demand. Moreover, because protons are being directly hyperpolarized and detected, it is inexpensive and straightforward to perform (since expensive isotopic enrichment and heteroatom-specific instrumentation can be obviated) and thus is readily applied with conventional clinical MRI scanners. This Minireview describes the fundamentals of PHIP for production of HP gases,[29] selected recent developments to extend the lifetime of the HP state through the use of the long-lived spin states (LLSS),[30] and HP gas application for void space imaging, remote sensing, time of flight imaging, and micro-fluidic imaging.

In all cases, the separation from other compounds required for hyperpolarization processes (e.g., Rb in case of SEOP of HP ^{129}Xe, free radicals in the case of DNP, and homogeneous or heterogeneous catalysts in the case of PHIP) is readily achievable, and experiments can be performed with HP gases in a chemically pure form.

2. Fundamentals of Noble Gas Hyperpolarization

2.1. SEOP

The most commonly employed method for generating HP noble gases is spin-exchange optical pumping (SEOP). The development of SEOP is rooted in the pioneering work of Kastler,[31] who was recognized with the Nobel Prize in physics for demonstrating that electronic spin order can be created in alkali metal vapors using circularly polarized laser light. Later Bouchiat, Carver, and Varnum[32] showed that the addition of ^3He to the gas mixture permitted helium nuclear spins to be polarized by spin-exchange collisions with the optically pumped alkali vapor atoms-work that was extended to ^{129}Xe by Grover.[33] The rich physics of SEOP has been extensively explored by Happer, Cates, Chupp, Walker, and many others (e.g., refs. [4, 17b, 34]), ultimately leading to the ability to produce large quantities of HP noble gases with nuclear spin polarization levels approaching unity for use in a variety of applications-including those described throughout this Mini-Review.

The underlying phenomenon of SEOP has been reviewed extensively elsewhere,[4,35] but can be briefly described as follows (Figure 1): First, a heated alkali metal vapor is irradiated with resonant circularly polarized light. Angular momentum conservation results in population being driven from appropriate spin-state ground states (e.g., $mJ=-1/2$ with $\sigma+$ light, neglecting nuclear spin degrees of freedom). The ground-state levels are repopulated at roughly the same rates, resulting in depletion of one-spin state and population accumulation in

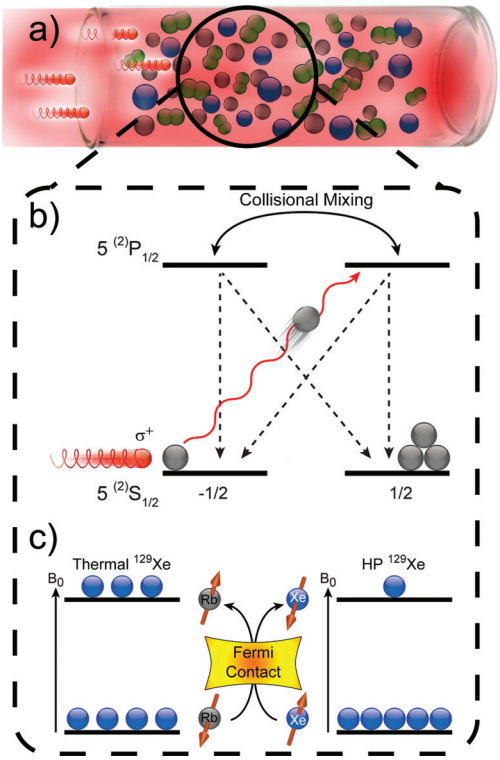

Figure 1. Schematic representations of SEOP.[2b,4] (a) SEOP cell containing a noble gas (here, Xe), buffer gases (e.g. N_2), and a small quantity of vaporized alkali metal (here, Rb); the cell is irradiated by circularly polarized laser light that can be absorbed by the alkali metal atoms. (b) The first step of SEOP: in order to conserve angular momentum, photon absorption results in selective population depletion from one Rb ground electronic state (neglecting Rb nuclear spin for simplicity). Although gas-phase collisions work to equalize the excited-state populations (and hence, the ground-state repopulation rates), continuous depletion of one state by the laser leaves the alkali metal vapor electronically spin-polarized. (c) The second step of SEOP: Gas-phase collisions occasionally allow spin order to be transferred from the alkali metal atom electrons to the noble gas nuclei via Fermi contact hyperfine interactions, thereby hyperpolarizing the noble gas over time. Reproduced with permission from Ref. [2b] John Wiley & Sons, Ltd., 2015.

the other-rendering the alkali metal vapor electronically spin polarized. Gas-phase collisions then transfer polarization from the electrons of the alkali metal to the spins of the noble gas nuclei via Fermi-contact interactions.

This process is allowed to continue so that the nuclear spin polarization can accumulate over time, ultimately yielding a steady-state nuclear spin polarization given by Equation (1):

$$P_N = \langle P_{AM} \rangle \cdot \left(\frac{\gamma_{SE}}{\gamma_{SE} + \Gamma_N} \right) \quad (1)$$

where $\langle P_{AM} \rangle$ is the spatially averaged polarization of the alkali metal vapor, Γ_N is the noble gas nuclear longitudinal relaxation rate ($1/T_1$) in the optical pumping cell, and γ_{SE} is the spin-exchange rate (i.e., the rate at which polarization can be transferred from alkali metal to the noble gas).

Although the vast majority of SEOP experiments have employed the spin $I=1/2$ noble gas isotopes ^{129}Xe and ^{3}He, the quadrupolar species ^{21}Ne ($I=3/2$),[36] ^{83}Kr ($I=9/2$),[37] and ^{131}Xe[38] ($I=3/2$) can also be polarized via this method. For the alkali metal vapor, Rb is most-commonly employed for practical reasons-including its low melting point[39] (facilitating vaporization) and the availability of high-powered lasers resonant with its D_1 transition;[40] however, K and Cs are also utilized (particularly for ^{3}He[41] and ^{129}Xe,[42] respectively).

Technological developments for SEOP have been extensively reviewed elsewhere,[35] and only a brief description is given here. Devices for preparing HP noble gases may be grouped into two types: "stopped-flow" and "continuous-flow". In a stopped-flow device,[43] a batch of a desired gas mixture is loaded into an OP cell (which contains a quantity of alkali metal) and is heated and optically pumped with a laser; once the gas is hyperpolarized, OP is stopped and the gas is transferred to the sample (usually after the cell has cooled to condense the alkali metal); alternatively, multiple batches may be systematically polarized and collected to accumulate the HP gas prior to transfer. In a continuous-flow device,[44] a desired gas mixture is allowed to flow from its source continuously through a heated cell while it is irradiated by the laser; the flow rate is chosen to allow sufficient average residency of noble gas atoms in the cell to enable the gas to be hyperpolarized "on the fly". The HP gas mixture can then either be directed into the sample or a cryo-condenser (to collect the otherwise-dilute HP noble gas and deliver it purely and with high density, following sublimation).[44a]

All of the noble gas isotopes are amenable to the stopped-flow design,[38,43h,i,45] whereas the relatively high spin-exchange rates and facile cryo-storage of ^{129}Xe's polarization[46] make it the best choice for use in a continuous-flow device. Both device designs have evolved considerably over the years, achieving ever-greater gas polarizations and production amounts/throughputs-benefiting in particular from the advent of compact, high-power, relatively low-cost light sources embodied by spectrally-narrowed laser diode arrays.[40,43e,g,44f,47]

2.2. Other Methods for Hyperpolarizing Noble gases: MEOP, "Brute Force", and DNP

In addition to SEOP, HP noble gases can be prepared by metastability exchange optical pumping (MEOP), "brute force", and dynamic nuclear polarization (DNP), and we briefly describe these approaches here.

In MEOP,[48] an electrical discharge is used to create metastable (electronically excited) atoms in a dilute gas. The unpaired electrons of these metastable atoms can be spin-polarized via optical pumping with a laser. The angular momentum of the electron spin may then be transferred to the nuclear spin of another gas atom in the cell during a metastability-exchange collision. The process is allowed to continue until a bulk nuclear spin polarization develops across the cell. Finally, a pump is used to compress the HP gas to a sufficient density prior to use.[49] MEOP works well for ^{3}He[48] and has been highly effective at producing clinical-scale amounts for biomedical imaging experiments (e.g., [50]); MEOP is generally less effective for the heavier noble gas isotopes because of stronger relaxation mechanisms.[51]

Next, to understand the so-called brute-force (BF) approach, one should first consider the relation determining the equilibrium ("thermal") nuclear spin polarization (for $I=1/2$ nuclei), see Equation (2):

$$P_N^{eq} \doteq \tanh\left(\frac{\gamma\hbar B_0}{2kT}\right) \quad (2)$$

where γ is the nuclear gyromagnetic ratio, B_0 quantifies the strength of the magnetic field, T is the absolute temperature, $\hbar$ is Planck's constant divided by 2π, and k is Boltzmann's constant. At room temperature and in a typical superconducting magnet, P_N^{eq} will be $\approx 10^{-5}$–10^{-6}. Thus, if the sample temperature were lowered to milli-Kelvin temperatures (and enough time were allowed for the nuclear spins to relax to their new equilibrium conditions), the nuclear spin polarization would exceed 10%. Although the approach can be time consuming, such BF approaches have used ^{3}He/^{4}He dilution refrigerators to polarize the nuclear spins in different substances, including noble gases.[52]

Finally, noble gases can also be hyperpolarized via DNP.[53] Here, the approach is essentially the same as that of dissolution DNP (d-DNP), introduced by Golman and co-workers in 2003.[1c] Briefly, the approach requires the substance to be hyperpolarized (here, ^{129}Xe) to be mixed in a glassy frozen matrix containing molecules with unpaired electron spins (e.g., a stable radical or a photoinduced, non-persistent radical).[53c] With the matrix placed at very low temperatures (~1 K) and at high magnetic field (several T), the unpaired electrons obtain a near-unity spin polarization. The matrix is then irradiated with microwaves in order to drive the high spin polarization to surrounding nuclei in the matrix, allowing a high bulk nuclear spin polarization to accumulate over time. The matrix is then rapidly warmed, sublimating the HP xenon as a pure gas-hence the name "sublimation DNP" given for this approach.[53b] Using DNP, polarization values of ~30% have been achieved in ~1.5 h,[53b] despite identified issues with a spin-diffusion bottleneck between electron and ^{129}Xe spins.[53a] Although the amounts and polarization values achieved thus far with DNP are not as high as corresponding values achieved with SEOP, the advantages are the increasing availability and general applicability of dissolution DNP polarizers in biomedical facilities-including Oxford's HyperSense[1c] and more recently, GE Healthcare's SPINlab.[54]

2.3. The Rise of Magnetic Resonance Applications of Hyperpolarized Noble Gases

Prior to finding their way into magnetic resonance, HP gases found their first applications in fundamental physics experiments (work that of course continues, see for example, refs. [55, 56]). And although the portions of this Mini-Review that are dedicated to HP noble gases are largely concerned with biomedical applications of ^{129}Xe, the first MR applications actually involved studies of materials (as well as investigations of the use of HP ^{129}Xe as a source of hyperpolarization for other spins).

Soon after the demonstration of ultra-long ^{129}Xe relaxation times for frozen solid xenon,[46] Pines and co-workers used HP ^{129}Xe NMR to probe the surfaces of powdered substances[43a] (and high-field gas-phase spectroscopy was also demonstrated by performing SEOP within an NMR magnet).[42a] Soon afterwards, the exquisite sensitivity of the ^{129}Xe chemical shift was investigated for probing surfaces of a number of porous materials and particles[57]-as was the ability to transfer the ^{129}Xe hyperpolarization to the nuclear spins of other substances.[58] The advent of continuous-flow production of HP ^{129}Xe[44a] was soon applied to greatly facilitate studies of materials surfaces,[59] including under conditions of magic angle spinning.[60] Since that work, HP xenon has been used to study diffusion in confined spaces or porous media;[61–63] image such systems as a function of gas flow[64] or ^{129}Xe chemical shift;[65] or spectroscopically probe single-crystal surfaces,[66] liquid crystals,[67] or combustion processes.[68] However, the greatest body of materials-related work has concerned the effort to probe void spaces and surfaces in microporous or nanoporous materials with HP ^{129}Xe, thereby providing information about pore size, pore shape, and gas dynamics in: nanochanneled organic, organometallic, and peptide-based molecular materials[69] (including in macroscopically oriented single crystals);[70] multi-walled carbon nanotubes;[71] gas hydrate clathrates;[72] porous polymeric materials and aerogels;[73] metal-organic frameworks;[74] calixarene-based materials and nanoparticles;[75] organoclays;[76] mesoporous silicas;[77] and zeolites and related materials[78]—efforts that have been aided by computational studies of xenon in confined spaces (e.g., ref. [79]). For a more in-depth review of HP ^{129}Xe in microporous and nanoporous materials, see ref. [80].

Indeed, ^{129}Xe has found the widest NMR/MRI application of the HP noble gases-a fact that is at least partially due to its significant natural abundance (26.44%) and ready recoverability from air during oxygen production. While ^{3}He does have the advantage of a roughly three-fold greater gyromagnetic ratio, its weak chemical shift dependence and lack of significant interaction with other substances make it a poor probe of other substances. More importantly, the lack of natural abundance (most ^{3}He comes from tritium decay) will limit the future use of this isotope for wide-scale magnetic resonance applications.[81] The rapid relaxation suffered by the quadrupolar isotopes (^{21}Ne, ^{83}Kr, and ^{131}Xe) presents a challenge for most HP NMR applications, although as pointed out by Meersmann and co-workers, the quadrupolar interaction also endows a unique sensitivity of HP ^{83}Kr to surface chemistry and local geometry that can be complementary to the information provided by ^{129}Xe chemical shift—a feature that can prove useful for probing porous materials, lung tissues, and other systems.[37,68b,82]

3. Clinical Application of Hyperpolarized Xenon-129 MRI

HP xenon-129 MRI (^{129}Xe-MRI) is an MRI modality first developed in the 1990s for enhanced lung imaging of ventilation and perfusion and regional information on gas exchange. It

has been used to image patients with a number of respiratory diseases, including asthma, COPD, and pulmonary fibrosis. In addition to its use in disease assessment and long-term management, in vivo gas-phase ^{129}Xe-MRI has the potential to provide imaging biomarkers of drug efficacy, which could be used to stratify treatment, improve patients' quality of life, and cut down healthcare costs. It can also be potentially employed by pharmaceutical companies to speed up decision-making in proof-of-concept studies in drug development.

3.1. From Mice to Men

Identified by British chemists William Ramsay and Morris Travers in 1898[83] (following their discovery of neon and krypton a few months earlier), xenon is a colorless and odorless noble gas. Xenon initially captured the attention of clinicians as a general anesthetic agent when Albert Behnke, a US Navy physician, investigated the cause for "drunkenness" observed in deep-sea divers.[84] Interestingly, Behnke also happened to be the clinician who had studied the anesthetic effects of nitrogen and helium in humans.[85] It was Lawrence et al.[85] who first published experimental data on the general anesthetic effects of xenon with mice as their test subjects. It took clinicians 5 years to put xenon to use in clinical settings,[86] and xenon has continued to be used as a general anesthetic since.

3.2. The Motivation for Hyperpolarized Xenon-129 MRI

The next major clinical application of xenon-129 came in 1994 in the form of its use as an inhalational contrast agent for magnetic resonance imaging (MRI).[87]

Plain radiograph and computed tomography (CT) are currently the main modalities used to image the lungs in clinical settings. Despite their ability to provide detailed anatomical data, in particular with high resolution CT, their main drawbacks are the risks involved with repeated radiation exposure and the inability to provide physiological information on regional lung function. Although conventional MRI has been a game-changer in both neuro and hepatic imaging, its dependence on the protons of water molecules in tissue to provide nuclear magnetic resonance (NMR) signal[87] has meant that it is of little value in imaging the lungs due to poor image quality because of three factors: 1- low proton abundance within the lung parenchyma, 2- air-tissue interface causing magnetic field heterogeneity, and 3- image degradation secondary to cardiac and respiratory motion.[88]

The NMR signal strength of a given species depends on its nuclear spin, that is, polarization, concentration, and the volume of the element. Except for those in water and fat, the concentrations of all other protons and nuclear species are too low to be of use in conventional MRI. However, hyperpolarization can be used to overcome the otherwise low detection sensitivity for low-concentration spins. For example, by delivering HP ^{129}Xe to excised mouse lungs, Albert and colleagues were able to obtain improved MR lung images compared to those obtained with conventional MRI.[87]

3.3. Hyperpolarized Xenon-129 MRI—There and Back Again

HP xenon-129 MRI of human lungs, which are obviously much larger than those of mice, proved challenging; it took physicists three years following Albert's paper in 1994 to be able to publish data on human studies.[89] The challenge was due to the need to produce much larger quantities of HP ^{129}Xe and to achieve adequate levels of polarization. Furthermore, conventional MR imaging sequences had to be modified as the polarization of the noble gas is non-renewable, and some polarization is lost every time an MR excitation pulse is applied.[90] These issues led to a shift in interest from ^{129}Xe to helium-3 (^{3}He), a fellow noble gas, whose larger gyromagnetic ratio and larger achievable polarization compared to ^{129}Xe at the time allowed for better signal intensity and image resolution for a given amount of HP gas.[91]

Interest in ^{129}Xe was reignited in the early 2010s; this resurgence was due to the fact that contrary to ^{129}Xe, which is naturally occurring, ^{3}He is a byproduct of tritium decay. ^{3}He had become scarce as the US sequestered ^{3}He for ^{3}He-based neutron detectors for national security, leading to extremely low availability of ^{3}He for scientific research and an exponential rise in its price.[91b] As a result, it was unlikely that ^{3}He-MRI would become a routine imaging modality in clinical settings, and so interest in ^{129}Xe-MRI was rekindled.

3.4. Safety & Tolerability Profile in Patient Groups

Over the past two decades, ^{129}Xe-MRI has been improved and utilized in imaging a wide range of respiratory diseases, including asthma,[92] chronic obstructive pulmonary disease (COPD),[92b,93] cystic fibrosis (CF),[92a] and pulmonary fibrosis.[94] Studies specifically designed to investigate the safety and tolerability of ^{129}Xe-MRI have not shown major common side effects in various patient groups, including those with asthma,[92a] and mild-moderate COPD,[92a,95] with light-headedness of very short duration as the main reported minor side effect.

3.5. Ventilation Imaging

Ventilation imaging provides valuable clinically relevant information relevant to regional lung function. Regions with normal ventilation typically appear bright and homogenous on ^{129}Xe-MRI, and in a healthy subject with normal lung function, both lungs show relatively homogenous ventilation except for two regions (as seen in Figure 2 and discussed in the caption). In those with diseased lungs where regional ventilation is impaired, the abnormal regions will appear darker; these regions are called "ventilation defects".

Compared to healthy volunteers, ^{129}Xe distribution has been shown to be regionally heterogeneous with ventilation defects in a number of different patient groups, including those with asthma, COPD, and CF.[92a,93c,d] Ventilation imaging has also been shown to correlate with spirometry[93c] and CT findings[96] in patients with COPD.

Additionally, ventilation imaging has been used to assess the efficacy of drug therapy. Studying the impact of Salbuta-

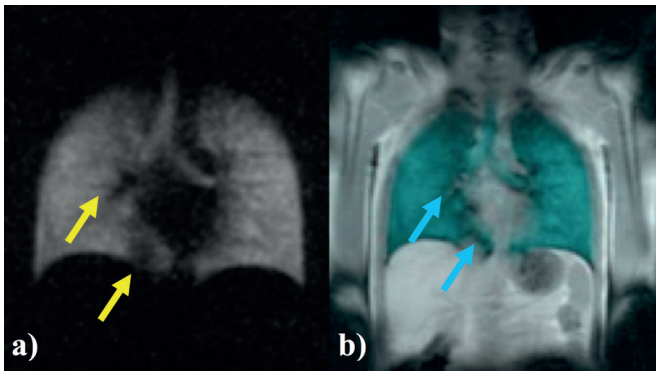

Figure 2. ^{129}Xe-MRI of a healthy volunteer. a) Coronal plane 25 mm slice ^{129}Xe-MR ventilation image of a healthy adult male, with ^{129}Xe appearing bright. The upper airways are visualized and delineated. b) Coronal plane 25 mm slice fused ^{129}Xe-MR ventilation and proton co-registration image, with ^{129}Xe appearing blue-green. The two black regions pointed out in the fused image (yellow arrows) are due to a diaphragmatic eventration and pulmonary vasculature, clearly defined on the fused image (blue arrows). J. Thorpe, B. Haywood, M. Barlow, S. Safavi & I. Hall—University of Nottingham (Unpublished work).

mol in patients with asthma, Parragra's group[92b] has reported a significant reduction in ventilation defects after Salbutamol administration.

Hence ^{129}Xe-MR ventilation imaging, although appearing simple, can be used to not only assess disease, but to also assess drug efficacy and monitor disease progression.

3.6. Diffusion Imaging

The apparent diffusion coefficient (ADC) of gas within lung is a function of alveolar size and geometry. This can be assessed using ^{129}Xe-MRI to characterize pulmonary microstructure at the alveolar level, as seen in Figure 3.

^{129}Xe-MRI derived ADC mapping has been shown to correlate well with pulmonary function tests,[93d,95] including total diffusing capacity for the lung (TLco). This is of important clinical significance, as it clearly illustrates the ability of ^{129}Xe-MRI to provide regional quantitative lung function data. In addition to its potential use in disease diagnosis, monitoring and assessing therapeutic drug efficacy, diffusion imaging can also be used to plan surgery, including tumor resection and lung volume reduction surgery for emphysema, as it can aid prediction of post-surgery lung function. The predicted post-surgery lung function is currently calculated using ventilation or perfusion scintigraphy and quantitative CT; however, there is a risk that scintigraphy, the most commonly used imaging modality, may underestimate post-operative lung function,[97] thereby, preventing the patient from undergoing potentially curative surgery.

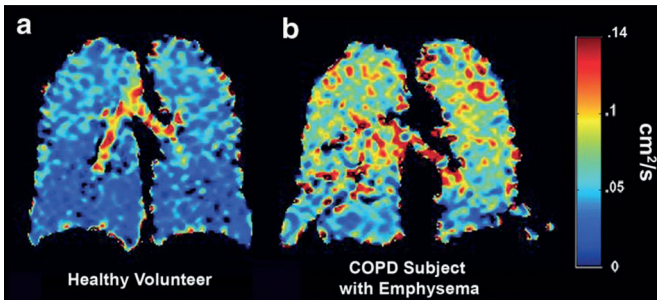

Figure 3. ADC map of a healthy volunteer and a patient with COPD. a) Healthy volunteer with a low mean ADC of 0.037 ± 0.021 cm^2 s^{-1}, indicating normal alveolar microstructure. b) Patient with COPD with high ADC values (0.068 ± 0.028 cm^2 s^{-1}) in the parenchyma, indicating alveolar destruction. Reproduced with permission from Ref. [95] John Wiley & Sons, Ltd., 2011.

3.7. Dissolved Phase Imaging

^{129}Xe (in contrast to ^{3}He) is highly lipophilic and soluble in biological tissues and thus is able to provide information on gas exchange and pulmonary perfusion, which can be particularly interesting in the context of functional lung imaging.[98] It is the associated persistent exchange of ^{129}Xe between the gas and dissolved compartments, each with its own different resonance frequencies, that is central to assessing gas exchange using ^{129}Xe-MRI.[99] Therefore, combined imaging of the gas phase ^{129}Xe and the dissolved phase ^{129}Xe would permit ventilation/perfusion (V/Q) imaging-and consequently a more direct mapping of lung function.[87] Hence, although ^{129}Xe-MRI initially lagged behind ^{3}He-MRI, developmentally, this capability provides another reason why ^{129}Xe-MRI is likely to be the pragmatic HP noble gas MRI modality of choice.

Although the majority of the inhaled ^{129}Xe remains in the airspaces, where it exhibits its primary gas-phase resonance, a portion dissolves in alveolar septa and crosses the alveolar-capillary barrier to dissolve in the blood. The resulting shift in the resonance frequency leads to the appearance of two additional distinct resonances: 1) the barrier resonance, and 2) the hemoglobin-associated ^{129}Xe resonance, as seen in Figure 4 (We note the intensity differences between the two spectra are due primarily to the variation in the amount and speed at which hyperpolarised xenon gas was inhaled by the two vol-

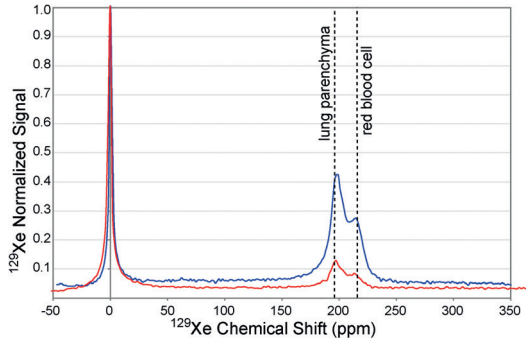

Figure 4. ^{129}Xe NMR spectra recorded from two healthy volunteers. Two dotted lines have been placed to represent the expected dissolved state peaks, the left most line representing the expected ~196 ppm lung parenchyma peak, and the right most line representing the expected 216 ppm red blood cell peak. S. Hardy, B. Haywood, M. Barlow, S. Safavi & I. Hall—University of Nottingham (Unpublished work).

unteers. As volunteers became more familiar with the breathing protocol, the improvements in both ventilatory image quality and dissolved phase signal/noise were noted). This transfer pathway is identical to that followed by oxygen; therefore, in addition to being a ventilation probe, ^{129}Xe is also a gas diffusion transfer probe.[94a]

The signal intensity of the dissolved phase ^{129}Xe is approximately 2% of that remaining in the alveolar spaces, which presents a challenge to obtaining good quality images.[94a] However, as the alveolar space, alveolar septa, and capillary blood are in dynamic exchange, it is possible to use nearly all of the inhaled gas to generate 3D images of dissolved ^{129}Xe in a single breath-hold, as demonstrated in a number of studies.[94a,100]

Another challenge is to distinguish between xenon dissolved in the alveolar septa and that dissolved in the blood. Various teams have used the chemical shift and the change in resonance frequency to distinguish xenon in these two compartments[98a,101] as the dissolved-phase ^{129}Xe signal splits into two distinct peaks in alveolar septa and blood. These methods, known as the Xenon Polarization Transfer Contrast (XTC)[98a,101b,c] and the Model of Xenon Exchange (MOXE),[101a,d,e] have been assessed in healthy volunteers[102] and patients with obstructive lung disease,[102a] with promising results.

Further testing these methods, Kaushik et al.[94a] hypothesized that there will be a reduction in ^{129}Xe signal intensity in the hemoglobin:alveolar septum ratio in patients with idiopathic pulmonary fibrosis (IPF), due to the thickening of the alveolar septa in this condition. MR spectroscopy was used to demonstrate the change in relative signal intensity in patients with IPF compared to healthy volunteers. The ratio was significantly lower in the IPF group compared to the healthy volunteer group, due to a 52% reduction in the hemoglobin signal and a 58% increase in the alveolar septa signal. There was a strong correlation between the hemoglobin:alveolar septum ratio and TLco. Therefore, this technique appears to provide a non-invasive measure of diffusion limitation and gas-transfer impairment.

These findings suggest that ^{129}Xe-MRI has the potential to detect subtle lung function deterioration before irreversible structural changes become apparent, providing clinicians with the chance to offer therapy (when available), at an earlier stage in order to delay, halt or reverse disease progression.

3.8. Neuroimaging

^{129}Xe-MR brain imaging is emerging as a distinct possibility. Just as xenon can be used as a gas exchange probe due to its ability to dissolve across the alveolar-capillary barrier, it can also be used as a cerebral blood flow (CBF) probe, as it can cross the blood–brain barrier and accumulate in the brain.[103] First utilized in its non-polarized form for CBF measurement using CT in 1982,[104] Swanson et al.[105] were the first group to publish data on brain MR imaging using HP ^{129}Xe as an inhaled neuroimaging contrast agent, albeit in rats. Animal studies have continued over the past two decades, using HP ^{129}Xe as both an inhalational[106] and injectable contrast agent.[107]

Diseased states have also been imaged in the rat model. Xenon signal in the brain is proportional to CBF, hence a decrease in the signal is expected to occur in areas of decreased CBF, such as those expected in ischemic stroke. Working on this principle, Zhou et al.[108] created a rat model of cerebral ischemia by using an intraluminal suture to occlude the middle cerebral artery, and demonstrated ^{129}Xe-MRI is able to detect the hypo-perfused area of focal cerebral ischemia, which was also confirmed on biopsy. Mazzanti et al.[109] further demonstrated the capacity of ^{129}Xe-MRI for functional neuroimaging by inducing pain in the rat's forepaw, and obtaining ^{129}Xe-MR images, which showed 13–28% increase in signal compared to the pre-stimulus images; these regions of increased signal corresponded to areas previously demonstrated by conventional functional MRI (f-MRI) as being activated by a forepaw pain stimulus.

It remains to be seen whether ^{129}Xe-MR neuro-imaging is feasible in humans and of value but developmental work is on-going.

3.9. Conclusion

Biomarkers of disease can be classified into diagnostic, prognostic, and theranostic. The ideal biomarker encompasses all groups, and ^{129}Xe-MRI has the potential to provide diagnostic, prognostic, and theranostic biomarkers.

4. Brown-Fat MRI using Dissolved Hyperpolarized ^{129}Xe

For biological MR applications, one of the most interesting properties of HP xenon is its high tissue solubility and its chemical shift sensitivity to its molecular environment. However, MR imaging and spectroscopy applications of dissolved-phase HP xenon have been limited to brain and lung tissues (as described in the sections above), as the concentration of dissolved-phase xenon in other tissues is rarely high enough to yield good signal after the typical single breath-hold protocol used for human studies. Neglecting nuclear spin relaxation and magnetization loss due to NMR pulsing, the time dependence of xenon concentration in tissues $C_i(t)$ is well described by the Kety–Schmidt, Equation (3):[110]

$$C_i(t) = \lambda_i C_a \left(1 - e^{-\frac{F_i}{\lambda_i}t}\right) \quad (3)$$

where λ_i, is the xenon partition coefficient between tissue and blood, C_a is the arterial concentration of the inert gas, and F_i is the blood flow to the tissue of interest. For most tissues, λ_i, which determines both the maximum concentration achievable in a given tissue and the time it takes to achieve maximum concentration, is close to unity.[111] However, F_i, which also determines wash-in rate, varies widely. For example, blood flow to the brain is very high ($\sim 0.5\ L\,min^{-1}\,kg^{-1}$) and the maximum xenon concentration in this tissue can be reached after a few seconds from the beginning of gas inhalation. On the other hand, while the solubility of xenon in fatty tissues is almost

20 times higher than in blood, because of the low tissue-perfusion (~0.01 L min^{-1} kg^{-1}), saturation can only be reached after several minutes. For HP ^{129}Xe gas, this is a clear limitation, as gas depolarization would limit the amount of detectable signal even under continuous HP xenon inhalation (because of short in vivo T_1 relaxation times).

It was recently shown that the intensity of the xenon dissolved-phase signal could reach much higher levels than in the brain in a tissue called Brown Adipose Tissue (BAT).[112] Brown adipose tissue is a fatty tissue found in most mammals, including humans, and its primary function is to generate heat through a process called non-shivering thermogenesis.[113] During stimulation of non-shivering thermogenesis in this tissue, intracellular triglyceride oxidation is decoupled from ATP production so that triglycerides are mainly burned to produce heat. To support this metabolic activity, BAT is richly vascularized. During non-shivering thermogenesis, tissue perfusion increases by several fold as blood flow is needed to support the tissue's oxygen demand and to quickly dissipate the heat produced.

Aside from its thermoregulatory function, BAT has recently gained a great deal of interest because of its presumed role in the regulation of body weight and blood glucose level. For example, a series of studies in rodents have clearly shown that BAT function can directly regulate body weight and improve insulin sensitivity.[114] However, the detection of this tissue still remains a challenge, especially in humans,[115] where it is sparsely distributed and not easy to detect by standard MR techniques. In the paper by Branca et al.,[23] a strong enhancement of the intensity of the xenon-dissolved phase signal was reported in mice inhaling HP ^{129}Xe right after stimulation of non-shivering thermogenic activity in BAT, an effect which was ascribed to the strong enhancement in blood flow to BAT.[116] Blood flow to this tissue during stimulation can reach values as high as 5 L min^{-1} kg^{-1},[116] considerably increasing xenon wash-in rate and allowing it to reach an in-tissue concentration of tens of mM. Since the increase in blood flow is specific to brown fat cells, background free maps of this tissue could be generated.

More interestingly, it was also shown that xenon chemical shift information can provide a measure of the relative tissue hydration and tissue temperature. Specifically, two major peaks were observed in these studies. One signal, at ~197 ppm, corresponds to xenon dissolved in cell cytoplasm/blood, and one signal at ~190 ppm corresponds to xenon dissolved in the lipid droplets of the tissue. The lipid-dissolved peak was shown to have a temperature-sensitive chemical shift (−0.2 ppm °C^{-1}), which enabled direct measurement of the increase in tissue temperature (Figure 5) during non-shivering thermogenesis.[23] In addition, during non-shivering thermogenesis, a relative decrease of the lipid-dissolved phase peak was observed with respect to the cytoplasm/blood peak, yielding direct evidence of this tissue's oxidative metabolism of internal triglycerides.

More recently, the feasibility of BAT detection in humans during a single breath hold of HP xenon was demonstrated, with validation by FDG-PET.[117] As in mice, a strong increase in the lipid dissolved xenon signal was seen in the same glucose-avid area of the supraclavicular fat depot. More interestingly, xenon spectra showed, in addition to the lipid-dissolved phase peak, a nearby peak around 200 ppm that was attributed to xenon dissolved in red blood cells (RBCs), a signal that provided direct evidence of the strong increase in tissue blood flow as the main drive for the increase in xenon tissue uptake.

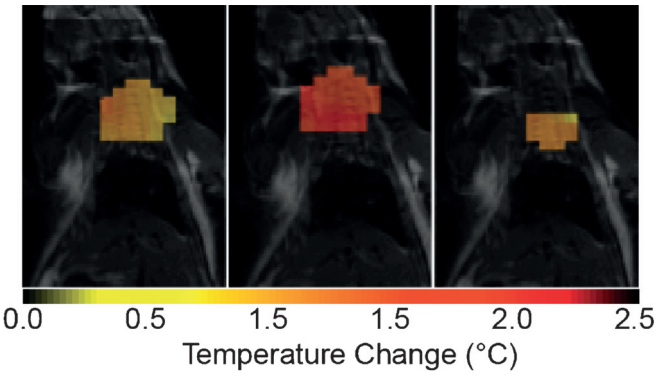

Figure 5. ^{129}Xe brown adipose tissue (BAT) temperature map overlaid on a sagittal ^{1}H image. These temperature maps were obtained by using the lipid-dissolved xenon signal as a temperature probe. The temperature coefficient of the lipid-dissolved xenon chemical shift was measured to be −0.2 ppm °C^{-1}.

By being a highly vascularized fatty tissue, BAT is clearly an easy target for the lipophilic xenon. In this case, HP ^{129}Xe gas MRI is a "one-stop shop" for human BAT studies as it is capable of providing both morphological and functional information.

5. ^{129}Xe Cages and Hyper-CEST MRI

5.1. Bound xenon and molecular hosts

In addition to the NMR study of HP Xe in the gas phase and the studies of tissue-dissolved Xe as described above, the affinity of xenon to reside in hydrophobic pockets enables additional insights. This phenomenon made xenon a tool for exploring binding sites on protein surfaces[2c] with some effort being put on spin polarization transfer to nuclei in nearby residues that form the catalytic site of enzymes. Hence, detection of proton signals with and without adding HP nuclei could identify the pocket-related residues.[111] Xe NMR spectra themselves can also show signals indicative of bound atoms. Such a population could either cause a shift of the dissolution peak or a distinct signal given the exchange rate would fall into the right regime.[112] An example are red blood cells[113] where the signal of "bound" Xe is ascribed to the interaction with hemoglobin.[118] Several experiments first used lyophilized protein powder samples, for example, of lipoxygenases.[119] NMR of dissolved Xe has been applied to identify binding pockets of lipid transfer protein,[120] and for observation of conformational changes in maltose binding protein,[121] and chemotaxis Y protein.[122] Besides specific site affinity for native structures, protein engineering also allowed for the design of conformation-sensitive binding pockets as demonstrated with the ribose binding protein.[123]

The binding of Xe to synthetic hosts where the cavity has a simpler design than in proteins can be even more pronounced. α-cyclodextrin[124] still comes with fast exchange but cucurbit[*n*]urils[125] (CB*n*, $n=5$, 6) show distinct peaks for bound Xe, as do cryptophanes, a family of molecular cages with some members that show rather high Xe affinity ($K > 10^3\ M^{-1}$).[126] It has been shown that different members of this group show distinct signals of bound xenon (Figure 6a). In particular cryptophane-A, CrA, is often used for conferring a distinct chemical shift to bound Xe ca. 130 ppm upfield from the signal of free Xe in aqueous solution.

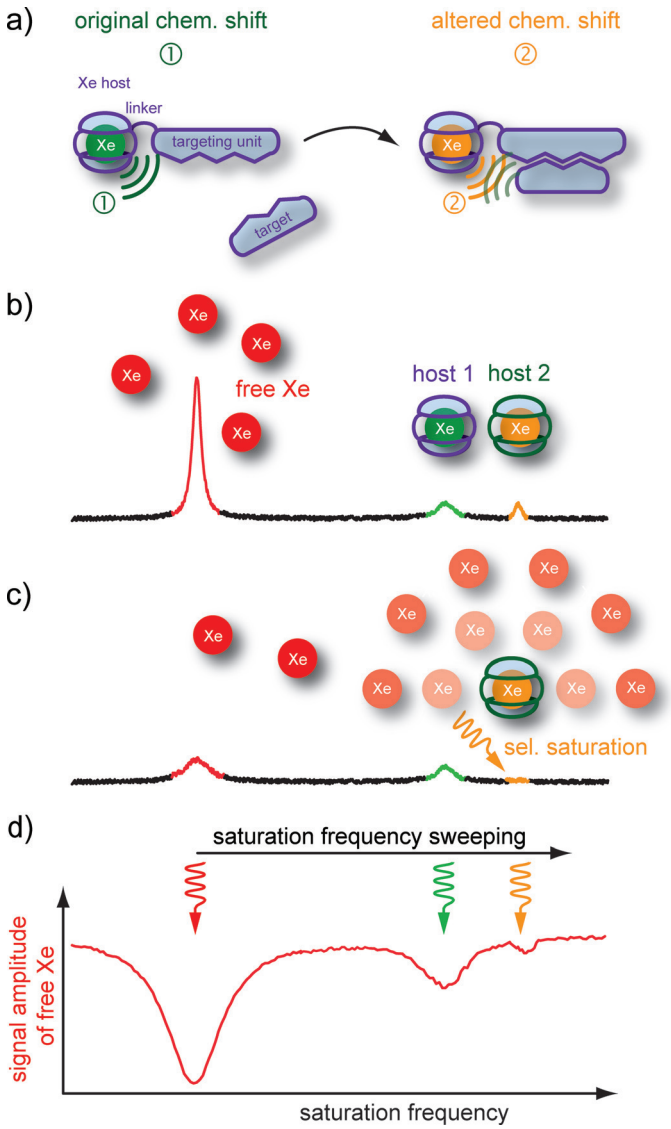

Figure 6. Caged Xe biosensor concept, and Hyper-CEST detection. a) Different Xe hosts confer different chemical shifts to the bound atoms that enable readout at distinct resonance frequencies. b) Xe inside a molecular host changes its resonance frequency upon binding to a target structure. c) Selective Hyper-CEST saturation at one of these frequencies causes a cloud of depolarized Xe around the respective host. The reduced signal from free Xe represents an amplified information from the small amount of cages. d) Sweeping the saturation pulse over a certain frequency range and subsequent observation of the magnetization from free Xe yields a Hyper-CEST spectrum for comparing the performance of different hosts.

5.2. Xenon biosensor concept

These molecular cages triggered the field of Xe biosensors where (for example) a variant of CrA is used as the NMR-active reporter being tethered to a binding unit to reveal the presence of a certain analyte (Figure 6b). The first implementation was shown with the biotin–avidin system.[127] This original publication also introduced the multiplexing option that this concept offers. This feature is inherent to the different cage types (like in Figure 6a), but also small chemical modifications on the cage, for example, deuteration,[127b] already provide a host-guest system with a different resonance frequency. Thus the combination of different hosts with different targeting units would allow for detecting multiple analytes simultaneously.

The sensing capability initially relied on a change in chemical shift and direct detection of the bound Xe signal-a concept that was later partially revised due to anticipated loss of spectral resolution in cells and live animals. Optimization for this concept included first and foremost increasing the Xe affinity and maximizing the detected chemical shifts. It is obvious that the cage size impacts the binding constant as illustrated in a comparative review,[128] but substitutions on CrA and cryptophane-111 can also increase the affinity.[129] Understanding the details behind the complexation of Xe revealed induced fit properties[130] and displacement of water[131] as contributing forces. The linker length between cage and targeting unit is a critical parameter for enabling the right balance between sufficient mobility required for narrow resonances and desired surface contact with the target to shift the signal.[132] Another relevant aspect of cryptophane-based sensors is the poor water solubility of the host. While many cages were first characterized in organic solvents, various synthesis studies succeeded to improve solubility.[129c,131,133]

5.3. Hyper-CEST signal amplification

The focus on the binding properties somewhat shifted with the advent of MR imaging protocols for such sensors. The low concentration of caged atoms (typically $<10^{-5}\ M$) requires extensive signal averaging for conventional detection. Initial imaging applications were slow and limited to selected spatial dimensions.[134] To improve this situation, the chemical exchange of Xe became an important parameter. One method for enhanced sensitivity in spectroscopy applications uses selective read-out of the caged Xe signal while the pool of dissolved Xe serves as a polarization reservoir.[135] This principle was also used in imaging[136] but has its limitations due to the timing that comes with frequency selective excitation pulses with defined flip angles.

However, inverting the roles of the participating pools, that is, manipulating the dilute pool and detecting the abundant solution pool, enables significant signal enhancements. The method with selectively saturating the magnetization from the dilute pool (either through cw irradiation, or by using a train of shaped excitation pulses) and observing the signal decrease of the other pool (Figure 6c) is called chemical exchange saturation transfer (CEST), first introduced by Balaban and co-work-

ers.[137] Combining CEST with HP nuclei was first demonstrated by the Pines lab for an imaging application and coined Hyper-CEST.[138] With Hyper-CEST, host concentrations as low as ~10^{-8} M become accessible-even for imaging.[139] The effect strongly depends on the exchange rate and therefore it can also sense system parameters like ambient temperature.[140] The spectral dimension can be recovered by performing a series of experiments in which the saturation pulse is swept over a certain frequency range (Figure 6d), thus providing another method to sense parameters that influence the chemical shift.[141] It also preserves the multiplexing option mentioned early on.

5.4. Xe Biosensor Applications in Cell Biology

The improved detection limits for imaging made it possible to address problems under more biologically realistic conditions. To date, cryptophane-based sensors that use specific binding to the target have been implemented for sensing the enzyme MMP7,[142] nucleotides,[143] human carbonic anhydrase,[144] MHC class II,[145] zinc ions,[146] the glycoprotein CD14[147] and the receptors for integrin,[148] transferrin,[149] EGF,[150] and folate.[151] An indirect binding approach was pursued through in situ click chemistry with metabolically labeled cell surface glycans.[152] Conformational changes of the sensor induced by changes in pH represent an approach for stimulus-induced binding.[153]

As part of these studies, cell uptake and toxicity evaluations set the bar for target concentrations of functionalized hosts.[148,154] Xe itself passes the cell membrane[149] and does not require further attention to reach intracellular targets. Cell-penetrating peptides proved to be a valuable measure for achieving micromolar intracellular concentrations. However, they are not an absolute requirement since the hydrophobic character of CrA can mediate membrane association and therefore enables certain types of cellular labeling.[155] Sensors with highly specific binding motifs (e.g., antibodies[147,150] or bioorthogonal reaction partners)[152] only require sample-averaged concentrations of 10^{-8} M for MRI.

Critically, the membrane affinity of CrA can be clearly identified by a ca. 10 ppm downfield shift for Xe in membrane-associated CrA.[156] This property proved primarily useful to identify cell-associated cages in the first live-cell experiments.[149,155a] A closer look in combination with FRET data revealed partitioning coefficients on the order 10^2–10^3 for different membrane compositions.[157] This work also initiated a new class of Hyper-CEST experiments for investigating membrane fluidity and integrity: Due to the accelerated exchange, Xe signals from membrane-embedded cages do only differ marginally in chemical shift. However, build-up of the CEST effect can be very different depending on membrane fluidity. Comparative studies are possible when irradiating a pool of caged Xe at fixed saturation power and frequency but increasing saturation time. Evaluating the (multi-)exponential depolarization with an inverse Laplace transformation yields characteristic time constants for different environments.[158] The method called DeLTA (depolarization Laplace transform analysis) can also be used to discriminate cholesterol content and the onset of lipid domain fluctuations.[159]

5.5. Host Optimization

In order to explore a large chemical shift range of different sensors, the impact of metal ion chelation in close proximity to the cage provides a means to diversify signals.[160] Along this line, attached Gd-chelates can serve as relaxation switches for ^{129}Xe which are detachable through chemical reactions.[161] Regarding Hyper-CEST detection, improved efficiency depends on the exchange properties, which are sub-optimal for CrA. Faster exchanging hosts such as CB6[162] and CB7[163] are currently under investigation. Their binding properties for competitive guests must be taken into account but this versatile binding phenomenon on the other hand enables the option to implement detection of other guests via displacements approaches. An example is the mapping of lysine decarboxylase (LDC) activity where the enzymatic product cadaverine quenches the Hyper-CEST effect.[163] Related to this is an implementation of a sensor relay in which the cavity becomes accessible for Xe as soon as another host recruits the original guest from the CB6 cavity.[164] The macrocyclic host also allows construction of rotaxanes that keep the cavity blocked. Cleaving one of the rotaxane stoppers releases the thread and makes CB6 available for Hyper-CEST detection.[165] This recent design could serve as a development platform for various sensors based on cleavage reactions.

Many dilute targets will only be accessible with an increased number of CEST sites per targeting unit. For this purpose, multivalent carriers with 10^2–10^3 Xe hosts will be the right tool. They have been implemented with scaffolds such as bacterial phages,[150,166] viral capsids,[167] and liposomes.[168] Alternatively, nano-compartments absorbing small amounts of Xe gas can be used, one example being PFOB nanodroplets.[169] The first imaging experiments with the latter substance also included the first multi-channel read-out of different host classes.[155b] Similar host compartments such as gas vesicles[170] and bacterial spores[171] will be discussed separately in the following section.

5.6. Hyper CEST Analysis and Data Encoding

Stable and reproducible HP Xe delivery with shot-to-shot noise $<1\%$ achieved through temperature stabilization of the pumping cell[172] allows one to further investigate the predicted line-shape for Hyper-CEST spectra, that is, an Lorentzian.[173] Linked to this theoretical description is an approximation for the Bloch–McConnell equations that allows prediction of the build-up of the Hyper-CEST effect and quantification of the exchange parameters.[174] Comparison of hosts can then be done by using the gas turnover rate.[162b] The exchange dynamics also set the boundary conditions for maximum signal contrast and an orientation for optimum saturation parameters.[175] It is important to achieve the saturation transfer before the intrinsic T_1 relaxation dominates with its signal loss.

For imaging, the CEST information needs to be encoded as fast as possible. Fast imaging sequences can replace the original point-wise encoding[138] given that sufficient magnetization is available. Echo planar imaging (EPI) allows sub-second imaging,[139] with particular application to hyperpolarized imaging using variable flip-angle excitation in an approach called smashCEST. These rapid imaging approaches enable time-resolved studies, including the monitoring of diffusion.[139] Image quality can be improved by exploiting redundancies in the spectral domain[176] during encoding and post-processing. Spin-echo encoding is an alternative for cases where T_2* relaxation makes EPI encoding impractical.[155a] Interest in HyperCEST agents has led to the development of fast strategies for gradient-encoded CEST spectra at up to 40-fold reduced scan times.[177]

6. Genetically Encodable Hyperpolarized ^{129}Xe MRI Contrast Agents

Genetically encoded MRI reporters are contrast agents that can be produced by genetically transfected cells to enable the tracking of cells, imaging of gene expression, or sensing of specific aspects of cellular function. Among the advantages of these reporters over synthetic agents are that they can be introduced into cells using established gene-delivery techniques, avoid dilution with cell division, and that a large genetic engineering toolbox can be used to modify and optimize protein-based reporter performance. Furthermore, these agents leverage the recent boom in molecular biology methods to manipulate and deliver genetic materials to animals, such as transgenic mouse lines, viral therapy, RNA interference, and genome editing.

Most existing genetic reporters have been designed for ^{1}H MRI. Examples include enzymes or transporters that can act on synthetic contrast agents,[178] proteins that naturally contain paramagnetic metals, including ferritin,[179] MagA,[180] MntR,[181] tyrosinase,[182] and cytochrome P450,[183] and diamagnetic CEST agents such as lysine rich-protein,[184] human protamine sulfate[185] and proteins that alter water diffusivity in tissue.[186] Comparatively fewer contrast agents have been designed for heteronuclear MRI, all of them based on enzymatic or transporter interactions with ^{19}F compounds,[187] HP ^{13}C compounds,[187c,188] or ^{31}P substrates.[189] A major challenge of all of these agents is their relatively low molecular sensitivity, typically of the micromolar or higher order, which limits their range of in vivo applications. Several excellent reviews have been written on these classes of MRI reporters.[190]

Given the sensitivity gains of HP ^{129}Xe MRI and in particular HyperCEST, there is a strong incentive to develop genetically encoded MRI reporters acting on xenon. However, this prospect is challenging due to the weak interaction of xenon with most proteins. Xenon-binding proteins have been identified through X-ray crystallography, wherein xenon is used as a heavy atom marker to aide in structure elucidation,[191] and NMR, wherein the ^{129}Xe chemical shift can probe proteins' confirmation and ligand binding.[192] Examples of proteins shown to interact with xenon include myoglobin[193] and hemoglobin, maltose-binding protein[112] and lysozyme.[119] These interactions are attributed primarily to enthalpic Debye and London interactions, with a smaller entropic contribution from xenon dehydration as it enters a hydrophobic cavity.[192b] Unfortunately, although protein binding was shown to shift the resonance frequency of xenon by several ppm mM^{-1}, these proteins are not suitable as ^{129}Xe-MRI contrast agents because their xenon affinities (~10 mM) would require unrealistic quantities of protein to be present to achieve significant direct contrast, while their xenon exchange rates (dissociation constant ~10^5 s^{-1})[193] are too fast compared to the induced xenon chemical shift ($\Delta\omega \sim 10^3$–10^4 s^{-1}) to enable efficient HyperCEST contrast.

A major advance in the development of genetically encoded reporters for Xe-MRI was made in 2014, when Shapiro et al. reported that an unusual class of gas-filled protein nanostructures called gas vesicles (GVs) could produce efficient HyperCEST contrast at picomolar concentrations.[25] GVs, which evolved in photosynthetic microbes as a means to regulate buoyancy, comprise hollow gas compartments at hundreds of nm in size and possess a 2 nm protein shell that is permeable to gas but excludes liquid water[194] (Figure 7 a,b). Shapiro et al. showed that GVs can interact with xenon to produce HyperCEST contrast with peak saturation approximately 175 ppm upfield from dissolved ^{129}Xe (Figure 7 c,d). The large chemical shift separation enables the contrast to be extremely efficient, with

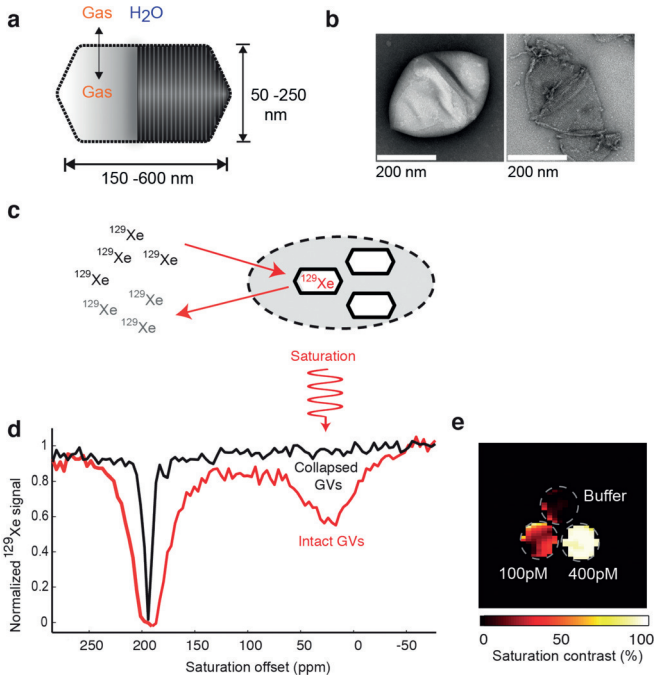

Figure 7. Gas vesicles as genetically encodable HyperCEST reporters detectable at pM concentrations. (a) Diagram of a gas vesicle: a hollow gas nanocompartment (solid shading) surrounded by a gas-permeable protein shell (ribbed shading). (b) Transmission electron micrographs of individual GVs purified from *Halobacterium* NRC-1 in their intact (left) and collapsed (right) state. (c) Diagram of ^{129}Xe CEST between bulk aqueous solvent (left) and GVs (hexagons) either in isolation or inside a cell (gray). (d) Frequency-dependent saturation spectra for intact (red) and collapsed (black) GVs. (e) Saturation contrast image of a three-compartment phantom containing 400 pM GVs, 100 pM GVs and buffer. Reprinted by permission from Macmillan Publishers Ltd: Nature Chemistry,[170] copyright 2014.

a GV detection limit in the picomolar range (Figure 7e), orders of magnitude lower than comparable proton contrast agents. Furthermore, GVs formed by different species of bacteria and archaea, in which these nanostructrues differ in size and shape, produce HyeprCEST saturation at different chemical shifts, thereby enabling multiplexed imaging. In their initial study, Shapiro et al. provided proofs of concept for GVs as antibody-functionalized markers of cancer cells and as reporters of gene expression in *E. coli*. In addition to GVs, other biological structures may be able to serve as HyperCEST agents. For example, bacterial spores, a dormant cellular state comprising a multilayered structure of ~1.5 μm size, were recently demonstrated for HyperCEST at a chemical shift 4.5 ppm downfield from aqueous xenon.[171]

The discovery of GVs as highly efficient biomolecular reporters for HyperCEST leads to several interesting questions and possibilities that merit further investigation. If we assume that an optimal CEST saturation can always be achieved with sufficient RF power and that the relaxation of ^{129}Xe is minimal during CEST experiment, then HyperCEST sensitivity is determined by (a) the chemical shift difference and (b) the exchange rate between the contrast-agent-bound and the dissolved ^{129}Xe spins.[195] Regarding the chemical shift, each GV has a several-attoliter gas chamber containing thousands of gas atoms or molecules, where ^{129}Xe atoms presumably experience an environment similar to gas phase, and consequently compared to the synthetic contrast agents, GV-associated ^{129}Xe chemical shift is usually closer to that of the gas phase. Intriguingly, the specific value of chemical shift appears to be genetically determined.[25] It will be interesting to study how this chemical shift relates to other genetically encoded GV properties, including their size, shape and aggregation state, and the extent to which these properties can be tuned at the genetic level. In terms of the exchange rate, when the Z spectra (i.e., the frequency-dependent saturation effects are visualized similar to conventional magnetization transfer spectra by plotting the water saturation (S_{sat}) normalized by the signal without saturation (S_0) as a function of saturation frequency) acquired with intact and collapsed GV are compared with those acquired with synthetic agents, both the GV-bound and the dissolved ^{129}Xe peaks appear to be broader, suggesting the exchange rate is in the intermediate regime. It will be interesting to define quantitatively the optimal RF saturation parameters for the specific exchange rate of GVs. On the molecular level, though the atomic-level structure of the GV wall has not been solved, some hypotheses have been proposed regarding the channels on the protein shell that allow gas exchange in and out of the nanostructure;[194b] it is possible that variation (natural or engineered) in the amino acid sequence of GV proteins could alter the permeability of these putative pores. Taken together, GVs present a wide dynamic range for ^{129}Xe chemical shifts and exchange rates, and these two properties are likely amenable to protein engineering for new and optimized forms of ^{129}Xe HyperCEST.

It is also worth noting that in addition to serving as HyperCEST reporters, GVs produce contrast in at least two complementary imaging modalities. First, they are the first genetically encodable imaging agents for ultrasound,[196] where their low density and high elasticity relative to surrounding media allows them to scatter sound waves. Secondly, their gas-filled interior, which has a different magnetic susceptibility from surrounding solution, allows GVs to produce ^{1}H MRI contrast in susceptibility-weighted imaging.[197]

The list of genetically encoded ^{129}Xe-based HyperCEST reporters has been recently expanded to include β-lactamase by Dmochowski and co-workers.[198] As a small protein encoded by a single gene, this reporter may be easier to use in some settings than GVs, albeit with somewhat lower molecular sensitivity.

7. Parahydrogen

Hydrogen exists in two nuclear spin isomers, denoted as *ortho*- and *para*-, corresponding to the nuclear triplet and singlet states, respectively: here parahydrogen corresponds to the states with an even rotational quantum number J whereas orthohydrogen corresponds to odd values of J. The ratio of the two isomers is determined by the Boltzmann thermal equilibrium for the given temperature, Figure 8.[199] For a more detailed discussion of the physics and applications of parahydrogen beyond the scope of this Minireview, we refer the interested reader to the 1935 book by Farkas on hydrogen[199] or various excellent discussions.[200]

Importantly, conversion between the two states occurs extremely slowly due to the transition being forbidden by the selection rules of quantum mechanics, leaving only statistically unlikely naturally occurring processes of sufficient energy (radiation, molecular collisions, etc.) to foment interconversion. Therefore, after its production (and provided lack of exposure to sources of paramagnetic impurities in the storage vessel), parahydrogen may be stored for long periods before use, as the relaxation rate of the parahydrogen back to room-temperature equilibrium can be on the order of months.[201] Production rates are significantly faster, however, since as discovered in 1929 by Bonhoeffer and Harteck, the use of paramagnetic catalysts (i.e., activated charcoal, nickel, hydrated iron(III) oxide) promotes establishment of Boltzmann thermodynamic equilibrium between *ortho*-H_2/*para*-H_2 states for a given temperature at greatly accelerated rates. In practice, normal hydrogen gas (i.e., equilibrium ratio at room temperature) consisting of 75% *ortho*- and 25% *para*- isomers is passed through chamber filled with paramagnetic catalyst and maintained at cryogenic temperatures, where the equilibration to the isomer ratio governed by the Boltzmann distribution occurs. For example, a parahydrogen generator operating at 77 K (obtained conveniently by a liquid-N_2 bath) yields a mixture with ~50% parahydrogen, whereas the designs based on cryo-chillers (e.g. $T \leq 20$ K) yield ≥ 99% parahydrogen (Figure 8).

8. Fundamentals of Parahydrogen-Induced Polarization (PHIP)

In 1986 Bowers and Weitekamp proposed a method for achieving very high nuclear polarizations using parahydrogen.[7a]

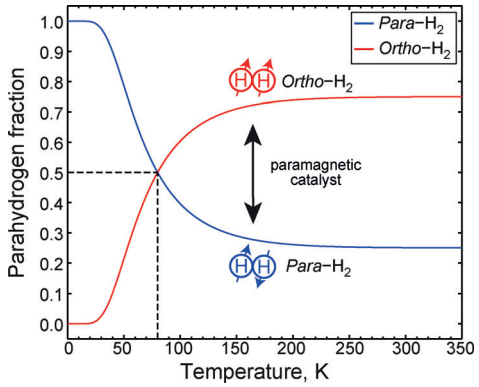

Figure 8. Parahydrogen conversion. Passage of H_2 gas over a paramagnetic catalyst, given sufficient contact time, converts the *ortho*-H_2 fraction to *para*-H_2 fraction as a function of temperature.

Dubbed PASADENA (Parahydrogen And Synthesis Allow Dramatically Enhanced Nuclear Alignment), the effect predicted strongly enhanced ^{1}H NMR signals for hydrogenation reaction products when unsaturated molecular precursors are hydrogenated with parahydrogen. Later they demonstrated the effect experimentally by hydrogenating acrylonitrile with parahydrogen using Wilkinson's catalyst.[7b] Anti-phase ^{1}H NMR multiplets were demonstrated for the reaction product, propionitrile, and for dihydride rhodium complex—the reaction intermediate. It was later realized that experimental demonstrations of the PASADENA effect had already been published,[202] but had been misinterpreted as chemically induced dynamic nuclear polarization.[7c] PASADENA and (the later discovered) ALTADENA[203] are collectively referred to as parahydrogen-induced polarization (PHIP).[11c] This seminal discovery of Bowers and Weitekamp opened up a new strategy for hyperpolarization of various compounds, and currently PHIP and its recent modification, SABRE (Signal Amplification By Reversible Exchange),[8] are used to obtain HP molecules with ^{1}H,[11c,200b] ^{13}C,[12] ^{15}N,[13d] ^{19}F,[14] and ^{31}P[15] nuclei in a hyperpolarized state.

Detailed explanation of the spin dynamics and chemical kinetics behind PHIP can be found in several comprehensive reviews.[11c,200,204] Here we briefly discuss the main principles of PHIP to qualitatively describe the phenomena discussed below. As an example, we take the simplest two-spin system. The two-spin system of the hydrogen molecule gives rise to four nuclear spin energy levels. As described above, three of these energy levels correspond to orthohydrogen, the state with total nuclear spin 1 (triplet state), whereas the remaining fourth energy level corresponds to parahydrogen (singlet state), the state with zero total nuclear spin. Transitions between singlet and triplet spin states are forbidden by symmetry;[7a] and the spin 0 parahydrogen is NMR-silent.

Bowers and Weitekamp's idea was to break the magnetic equivalence of two hydrogen nuclei by using parahydrogen in a hydrogenation reaction (Figure 9a), thus, making prohibited transitions allowed. Indeed, upon incorporation of a parahydrogen molecule into an asymmetric molecular precursor, the symmetry of the *para*-H_2 molecule becomes broken. This situation strongly depends on the magnetic field at which the hydrogenation reaction takes place. If hydrogenation is performed at high magnetic field B_0 (i.e., wherein the chemical shift difference between the two *para*-H_2-nascent protons, $\Delta\delta$, is much greater than the spin-spin coupling J between them ($\gamma\Delta\delta B_0 > 2\pi J$)), then the population of the singlet spin state ($\alpha\beta - \beta\alpha$) of *para*-$H_2$ is transferred to the population of spin states $\alpha\beta$ and $\beta\alpha$ of the formed weakly coupled AX spin system (PASADENA effect, Figure 9b).[7b] The NMR spectrum of the AX system populated in this way will contain four peaks grouped in two antiphase multiplets (Figure 9b).

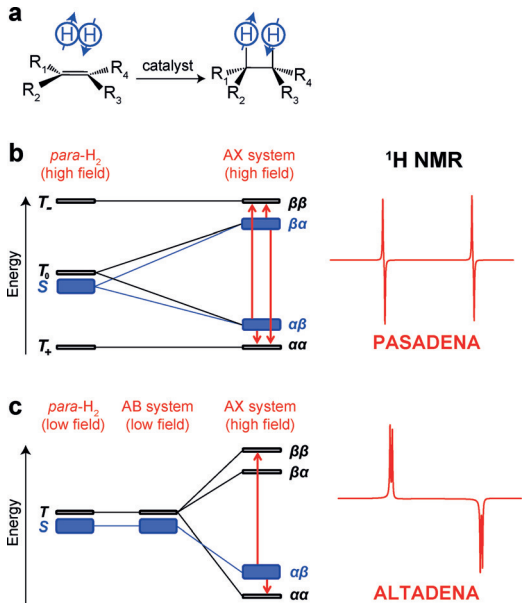

Figure 9. a) Molecular diagram of parahydrogen (*para*-H_2) addition to the substrate performed with a homogeneous or heterogeneous catalyst. b) PASADENA effect: nuclear spin energy level diagram of *para*-H_2 at high magnetic field (left). An AX spin system is formed upon pairwise addition of *para*-H_2 to the unsaturated substrate at high magnetic field and corresponding ^{1}H NMR spectrum is shown on the right. c) ALTADENA effect: nuclear spin energy level diagram of *para*-H_2 at low magnetic field (left). An AB spin system is formed after pairwise *para*-H_2 addition to the unsaturated substrate at low magnetic field. An AX spin system is obtained after adiabatic transfer of the reaction product from low to high magnetic field. The corresponding ^{1}H NMR spectrum is shown on the right.

Two lines (positive-negative or negative-positive, depending on the sign of spin–spin coupling constant J) in each multiplet are separated by J Hz in the case of isotropic liquids and/or gases.[205] The PASADENA-hyperpolarized organic molecules are typically manifested in ^{1}H NMR spectra as positive-negative multiplets, whereas multiplets for hydride intermediates are negative-positive, since J couplings are usually negative for metal hydrides.[206] Interestingly, the signal intensity of PASADENA spectrum is maximized when a 45° (instead of 90°) pulse is applied for signal acquisition, which may be shown using a density operator description of the PHIP process.[204]

On the other hand, if the hydrogenation reaction takes place at low magnetic field (such that $\gamma\Delta\delta B_0 \leq 2\pi J$; e.g., at the Earth's magnetic field), and afterwards the hydrogenation

product is adiabatically transferred to a high magnetic field, then there is a single state that is overpopulated, that is, $\alpha\beta$ *or* $\beta\alpha$-depending on the sign of the *J*-coupling constant between the nuclei (ALTADENA effect, Figure 9c).[203] In this case after a 90° pulse the spectral pattern will consist of four lines grouped in two "integral multiplets" simply corresponding to one spin "up" and second spin "down" state (Figure 9c).

In order to be able to observe PHIP for the molecule of interest several key conditions must be fulfilled:[11c]

1. The addition of parahydrogen to the unsaturated precursor should occur in a pairwise manner. Pairwise addition implies that two hydrogen atoms from the same H_2 molecule are included in the product molecule together as a pair, thus preserving spin correlation between the two proton spins.
2. The characteristic nuclear spin relaxation time for *para*-H_2-nascent protons should be longer than the time needed to complete the pairwise hydrogenation process.
3. The magnetic equivalence of the two correlated nuclear spins should be broken during the hydrogenation[207] or in the product of the hydrogenation reaction.[7b]

If all of the above-mentioned conditions are fulfilled, the product of the hydrogenation reaction will possess a non-equilibrium population distribution of its nuclear spin energy levels owing to either the PASADENA or ALTADENA process.

One should note that the final polarization of the hydrogenation reaction product does not depend on the magnetic field strength, and the polarization obtained by PHIP in principle can reach 100% (neglecting spin relaxation and/or decoherence).[7a,204] In principle, enhancement of the NMR signal can be as high as several thousand-fold above ordinary thermal signals from high-field NMR spectrometers and even a million-fold at low magnetic fields.

Since the hydrogenation reactions have a significant activation energy barrier, the key component of the system is a catalyst (Figure 9a), which (i) enables the hydrogenation reaction, and (ii) provides efficient pairwise addition of molecular hydrogen to the substrate. All hydrogenation catalysts can be classified as homogeneous or heterogeneous depending on their phase relative to the substrate. Homogeneous catalysts are present in the same phase as the to-be-hydrogenated substrate (typically, liquid phase), whereas heterogeneous catalysts are present in a phase different from the phase of the substrate (usually, a solid catalyst and a gaseous or liquid substrate). Since the first demonstration by Bowers and Weitekamp,[7b] homogeneous catalysts have become widely used to produce PHIP, which is reasonable: it is known that hydrogenation mechanisms using metal complexes can usually provide an efficient route for pairwise hydrogen addition. For a long time, the feasibility of using heterogeneous catalysts for production of PHIP was rejected based on the known mechanism of heterogeneous hydrogenation, that is, the Horiuti-Polanyi mechanism. According to Horiuti and Polanyi,[208] hydrogen molecules dissociate on metals (typically used as heterogeneous hydrogenation catalysts) and form a pool of randomly moving free hydrogen atoms, thus ostensibly not fulfilling condition 1 (pairwise addition) above.[209] Nevertheless, it was shown that various classes of heterogeneous catalysts, that is, immobilized metal complexes,[9a] supported metal nanoparticles,[28b] etc., can enable the PHIP effect. In the current minireview both classes of catalysts are considered.

9. Gases Hyperpolarized via PHIP

As mentioned in the introduction, MRI of gases suffers from poor sensitivity due to their low molecular density combined with the low thermal polarization of their nuclear spins. These problems can make it challenging to image gas-filled void spaces due to the very low signal-to-noise ratio (SNR) and the usually long signal-averaging times, which can be prohibitive for many clinical applications. HP noble gases[210] can be used to address these issues. However, the production of HP noble gases is relatively expensive, necessitating costly hyperpolarizer equipment. Moreover, imaging of HP noble gases requires a dedicated X-band channel (for the heteronucleus of interest) and radio-frequency probe, which are not standard features of clinical MRI scanners (although they are becoming increasingly prevalent). Therefore, production of non-toxic HP proton-containing gases via PHIP could be a promising alternative that avoids the above technical requirements of HP noble gases.

9.1. Production of Hyperpolarized Gases Using PHIP

Historically, experiments with parahydrogen were predominantly conducted in the liquid phase, wherein fluids hyperpolarized by PHIP reside in a solution along with a homogeneous hydrogenation catalyst.[200b] Heterogeneous catalysts can be used to separate the HP product from the catalyst.[29,211] At the same time, it is also possible to produce catalyst-free HP gases by combining the main advantage of homogeneous (high selectivity) and heterogeneous catalysis (easiest catalyst separation) by using gas-liquid biphasic hydrogenation. Utilization of a homogeneous catalyst dissolved in the liquid phase for biphasic hydrogenation of unsaturated gases with *para*-H_2 allows one to produce HP gas that is free from contamination by the catalyst. In the demonstration of this approach it was shown that the reaction product can return to the gas phase while retaining a significant degree of hyperpolarization.[212] This feature significantly extends the range of gases that can be hyperpolarized. It was shown that utilization of a simple experimental procedure allows one to achieve signal enhancements of 300 for propyne hydrogenation to propylene using the bidentate cationic complex $[Rh(PPh_2\text{-}(CH_2)_4\text{-}PPh_2)(COD)]BF_4$.[212] Another approach for HP gas production is the use of homogeneous catalysts based on a careful choice of the metal complex (homogeneous hydrogenation catalyst) in which the desired unsaturated substrate is coordinated to the metal center.[213] In that case hydrogenation of the substrate with parahydrogen allows the product to leave the metal center and to migrate to a different phase with preservation of the spin order of the two nascent protons derived from the *para*-H_2 molecule. Indeed, it was shown that PHIP-hyperpolar-

ized gas can be obtained in a catalysis-free regime using a chemical reaction with molecular addition of parahydrogen to a water-soluble Rh(I) complex carrying a payload of a compound with double (C=C) bonds.[213] Hydrogenation of the norbornadiene ligand leads to the formation of norbornene, which is expelled from the Rh^{I} complex to the aqueous phase, but due to its insolubility in water HP norbornene migrates from the solution to the gas phase (Figure 10).[213]

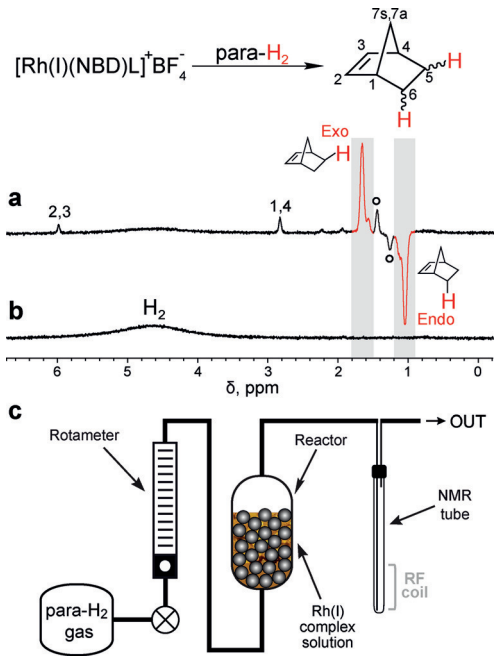

Figure 10. ALTADENA ^{1}H NMR spectra of a gaseous stream during bubbling of parahydrogen (a) and normal H_2 (b) through the solution of $[Rh(I)(NBD)L]^{+}BF_4^{-}$ in D_2O at 70–80 °C. The broad signal labeled "H_2" belongs to *ortho*-H_2 gas: the resonances labeled with open circles correspond to norbornane. c) Diagram of the experimental setup with the NMR detection performed in the high field. Reprinted with permission from ref. [213], Copyright (2014) American Chemical Society.

As soon as PHIP was successfully demonstrated in heterogeneous hydrogenations over immobilized[9a] and supported metal catalysts,[28b] the production of HP gases over these catalysts became an important area of PHIP-related investigations. Many different heterogeneous catalysts were used for the production of HP gases in the past eight years, with the aim to find the catalyst with the highest level of pairwise hydrogen addition for a given substrate.[29,214] Without doubt the utilization of a solid catalyst allows one to produce HP gases in the continuous-flow regime by passing a mixture of an unsaturated substrate with *para*-H_2 through the catalyst layer. In this approach, hydrogenation occurs at the Earth's magnetic field and corresponds to the ALTADENA[203] type of PHIP experiment. Note that the nature of the heterogeneous solid catalyst can have a significant impact on the polarization level, and titania-supported metal catalysts were shown to exhibit larger PHIP effects compared to metals on other supports.[215] The polarization level for HP gases produced over supported metal catalysts can be several percent,[28b,216] and it can change with the variation of the size of the supported metal nanoparticles.[217] Larger polarizations are observed for smaller Pt particles, but for Pd there is an opposite trend.

9.2. MRI of Hyperpolarized Hydrocarbon Gases

Continuous production of HP gases via heterogeneous hydrogenation paves the way to the potential practical applications for imaging of void spaces by MRI. The first experiments were related to MRI visualization of HP propane in a NMR tube with a cross-shaped partition or with a series of capillaries.[9b] For that work, a mixture of *para*-H_2 and propene gas was flowed through a reactor cell with the heterogeneous catalyst (e.g., Wilkinson's catalyst immobilized on silica). After that the product (HP propane gas) was transferred to the NMR magnet and the ALTADENA enhancement was evident in the MR images.

For both model samples, detection of the NMR signal of a thermally polarized gas did not produced observable images, whereas the use of PHIP-polarized propane gas allowed one to visualize the corresponding structures of the objects used in the experiments.[9b] Importantly, the demonstrated 300-fold signal enhancement in the gas-phase MRI is sufficient to image gases with a similar spatial resolution as that in corresponding liquid-phase MRI experiments. The subsequent development of the strategies for ^{1}H MRI visualization of both hyperpolarized (Figures 11 and 12) and thermally polarized propane gas

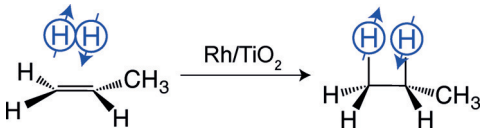

Figure 11. Heterogeneous pairwise hydrogenation of propene to propane with *para*-H_2 over Rh/TiO_2 catalyst with preservation of spin order of parahydrogen in the final HP product.

for high-resolution MRI applications allowed one to significantly decrease the imaging time. Compared to FLASH MRI[218] (Figure 12), the use of UTE MRI[219] decreases the total imaging time significantly, down to the regime sufficient for MRI of a patient within a single breath-hold in a future clinical translation. It was shown that utilization of UTE MRI makes it possible to obtain 2D images of thermally polarized propane gas with ca. 0.9×0.9 mm^2 spatial resolution in ca. 2 s (and potentially with better resolution for HP gases).[220]

Recently, HP propane gas produced by heterogeneous hydrogenation of propene over supported metal catalysts was utilized for 3D ^{1}H MRI with micro-scale spatial resolution ($625\times625\times625$ μm^3), large imaging matrix size ($128\times128\times32$) and short (17.4 s) image acquisition time.[215a]

Utilization of a fully deuterated substrate (propene-d_6) in the heterogeneous hydrogenation with *para*-H_2 permitted acquisition of a high-resolution 3D MRI image of flowing HP [D_6]-propane gas with $0.5\times0.5\times0.5$ mm^3 spatial and ~18 s temporal resolution (Figure 13 a).[221] It was shown that the signal-to-noise ratio in the 3D images of HP [D_6]-propane gas (Fig-

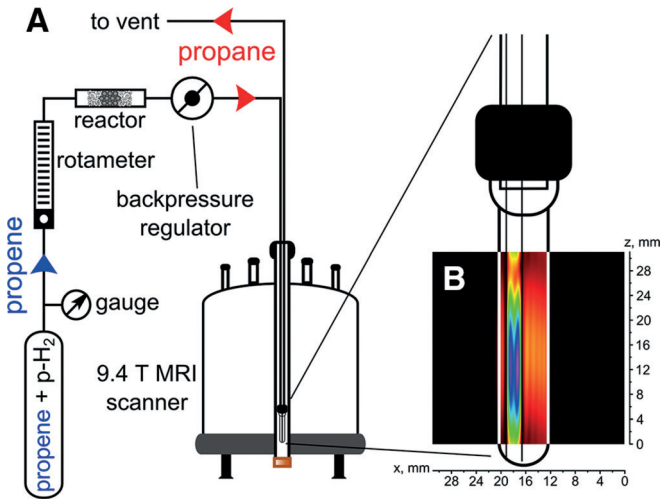

Figure 12. (a) Schematic representation of the experimental setup for using PHIP to produce HP propane via heterogeneous hydrogenation of propene with parahydrogen. (b) ^{1}H MRI FLASH image of HP propane flowing into a 10 mm NMR tube via 1/16 in. OD Teflon capillary. Note that the NMR tube is shown schematically and its length does not match the actual scale of the 2D MR image. Reprinted with permission from ref. [220].

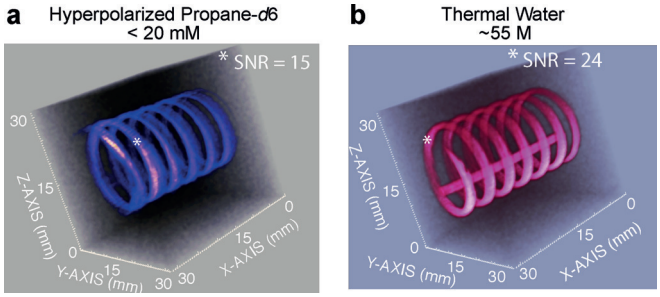

Figure 13. High-resolution 3D gradient echo (GRE) MRI at 4.7 T. a) 3D MRI of flowing HP propane gas (~20 mM concentration) with $0.5\times0.5\times0.5$ mm^3 spatial and 17.7 s temporal resolution and $32\times32\times32$ mm^3 field of view. b) The corresponding image of (stationary) thermally polarized tap water (55 M). Reprinted with permission from ref. [221], Copyright (2014) American Chemical Society.

ure 13a) and water (Figure 13b) are similar. This observation confirms that the utilization of a gas hyperpolarized by PHIP allows one to obtain MR images with quality similar to that obtained with water as the signal source.

Utilization of HP gases produced by PHIP is not limited only to void space imaging. Indeed, it was shown that a catalytic reactor positioned inside an NMR magnet can be imaged in situ during heterogeneous hydrogenation of propene to propane with parahydrogen.[28a] In situ MRI of a catalytic reaction allows one to visualize the regions in the catalyst layer where the hydrogenation reaction occurs. Importantly, based on the significant signal enhancement the velocity map for HP gas forming in and flowing through the catalyst bed was obtained.[28a]

Given the above results, PHIP is clearly becoming an important technique for signal enhancement in both basic science and biomedical MRI investigations. Moreover, the use of PHIP to produce HP gases can be useful for their potential utilization in medical MRI applications.

10. Remote-Detection MRI of Hyperpolarized Gases

MRI of gases in small voids, such as in porous media, microreactors, and microfluidic devices, suffers from particularly low sensitivity due to an additional exacerbating factor: low filling factor of the NMR coil, which may be less than 10^{-5} in some cases. While HP methods partially compensate for the low sensitivity, an additional sensitivity boost provided by alternative detection methods may be required. These methods include, for example, surface RF microcoils, RF microslots, and remote detection (RD), to name a few.[222]

In RD MRI,[223] encoding of spatial information and signal detection are performed with different coils in different locations (see Figure 14a). The encoding RF coil is a large coil around the whole sample, so that all spins can be excited. Signal detection is performed outside the sample with a much smaller and more sensitive RF coil, with an optimized filling factor.[224] The technique requires that the encoded spins are transported to the detector before the magnetization is fully relaxed, and it inflicts one additional dimension as compared to conventional MRI, because it is based on phase encoding only. Nevertheless, it provides a substantial sensitivity boost as an ultrasensitive detection solenoid may be hundreds of times more sensitive than the encoding coil.[225] Furthermore, the flow delivers spins

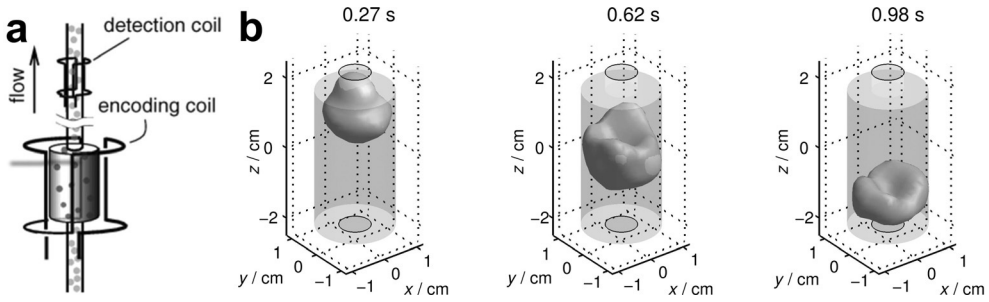

Figure 14. RD MRI of flow of HP ^{129}Xe through a rock sample. a) The rock sample is inside a large RF coil used to encode spatial information into spin coherences, and the signal is read out by a smaller and more sensitive coil around the outlet tubing, with optimized filling factor. b) 3D TOF images. The silhouettes represent the rock sample. TOF, i.e., the time instant the signal is detected after the encoding, is shown above the images. Reprinted with permission from J. Granwehr, E. Harel, S. Han, S. Garcia, A. Pines, P. N. Sen, Y. Q. Song, *Phys. Rev. Lett.* **2005**, *95*, 075503. Copyright (2005) by the American Physical Society.

from the different parts of the sample to the detector at different times, and this inherent time dimension can be utilized to produce time-of-flight (TOF) flow images.[226]

10.1. Time-of-Flight Flow Imaging with HP Gases

HP Xe is an ideal probe fluid in RD MRI experiments, because the T_1 relaxation time of ^{129}Xe can be extremely long, allowing correspondingly long transport times from the sample to the detector. HP Xe RD MRI has been used for imaging flow through porous materials,[223,227] rocks,[226] microfluidic devices,[225] and wood,[228] as well as for quantifying diffusion through membranes.[229] Figure 14b shows a remarkable example of 3D TOF images of HP Xe flowing through a rock sample. The shortest TOF image (TOF = 0.27 s) shows spins that were at the top of the encoding region, because they arrived first to the detector, and the longest TOF image (TOF = 0.98 s) shows the spins at the sample bottom.

Gaseous HP hydrocarbons produced by PHIP have been used in RD MRI experiments as well.[230] T_1 values for spins of hydrocarbons are typically much shorter (~1 s) than that of ^{129}Xe, limiting the transport time of fluid from the sample to the detector; however, if the sample coil and the detection coil are close enough and the flow rate is sufficiently high, the experiments are feasible. Because the gyromagnetic ratio and the natural abundance of ^{1}H is much higher than that of ^{129}Xe, the sensitivity in PHIP experiments may be greater.

As an example, Figure 15b shows 2D RD MR images of HP propane, which was produced by propene hydrogenation with *para*-H_2 over an Rh catalyst, flowing in a microfluidic capillary.[230a] Overall, the combined sensitivity gain provided by the RD scheme and PHIP was 48000-fold, and the experiments turned out to be one to two orders of magnitude more sensitive than the corresponding RD experiments with HP Xe. Comparison of the TOF images of a gas and a liquid (Figures 15b,c) nicely depicts different flow behavior of these phases; laminar flow of a liquid translates the encoded liquid molecules over a large distance (Figure 15c), whereas for a gas the three orders of magnitude faster diffusion causes efficient mixing of the flow lamellas, leading to a significantly less dispersed, plug-like flow behavior (Figure 15b).[230a,b]

Experiments with model microfluidic chips have supported the viability of the RD-PHIP approach for visualization of complex microfluidic geometries and flow quantification, Figure 16.[230a] Moreover, these experiments exposed the manufacturing imperfections of the chips. The gas flow in different channels varied in an irregular manner, and the signal amplitude profiles revealed an inhomogeneous distribution of the gas, implying that the channel depth varied from one channel to another.

10.2. Microfluidic Reactor Imaging

The natural ability of *para*-H_2 to participate in many important chemical reactions, including those performed with the use of microfluidic devices, opens an avenue for studies using HP gases. Combined RD MRI and PHIP methodologies in such studies were exemplified by the demonstration of catalytic reaction imaging of microscale catalyst layers.[230c] Tiny layers of heterogeneous Rh catalyst packed in thin capillaries (150–800 μm in diameter) served as model microfluidic reactors. It was shown that the RD-PHIP methodology can be used for visualization of mass transport and progress of gas-phase propene hydrogenation reaction inside the microreactors.

The white dashed rectangles in Figure 17 highlight the locations of the catalyst layers. The accumulation of produced HP propane with the distance that gas mixture travels inside the catalyst layer is visualized by the increased signal amplitude in the lower part of the reactor. It was shown that under the given conditions (relatively short travel times), the signal decay due to nuclear spin relaxation was quite insignificant, and the amplitude of the HP propane signal was directly proportional to reaction yield, allowing the determination of the rate of propene hydrogenation.

In addition, the experiments enabled the observation of gas adsorption effects in the microfluidic reactors during their in situ operation, and an elegant approach for quantifying the

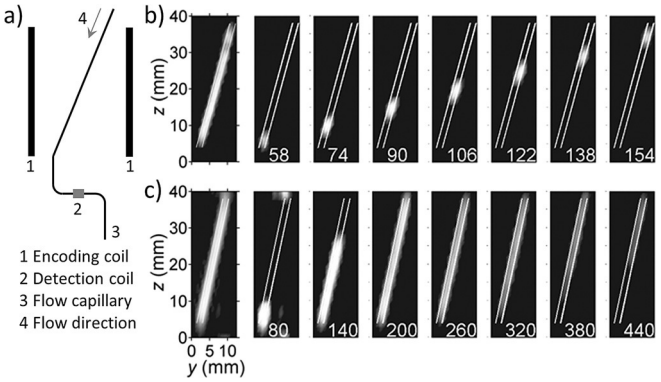

Figure 15. a) RD MRI setup of a simplified microfluidic system consisting of a capillary leading through the encoding and detection coils. TOF RD MRI visualization of (a) HP propane and b) water flow in the capillary (outlined in white), revealing much more extensive dispersion of liquid than that of gas molecules. TOF (ms) is shown at the bottom of the panels. The panels on the left are sums of the other panels.[230a]

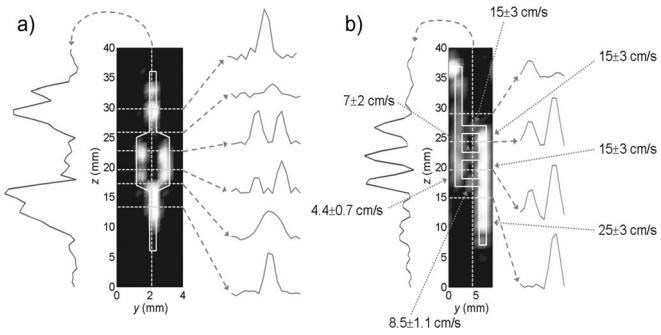

Figure 16. RD MRI of HP propane in microfluidic chips with a) a widened channel in the middle part and b) ladder-like channels (outlined in white). These images are the sum of the panels measured at different TOF instances, and they expose, e.g., manufacturing imperfections. Flow velocities extracted from TOF data are shown in b). Reproduced with permission from Ref. [230a] John Wiley & Sons, Ltd., 2010.

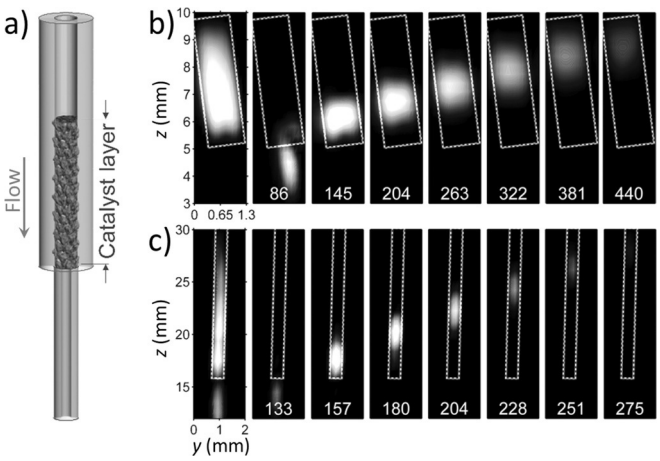

Figure 17. RD MRI visualization of reaction progress inside a catalyst layer packed in a thin capillary. a) Sample setup. 2D TOF images of HP propane resulting from the hydrogenation reaction in the reactors of a) 800 and b) 150 μm in diameter. The reactors are outlined by a white dashed line in the figures. TOF (ms) is shown at the bottom of the panels. The panels on the left are the sums of all other panels in each series.[230c]

amount of absorbed gas using RD NMR was proposed. The authors also introduced the concept of a microfluidic nuclear polarizer based on their findings about PHIP produced in the microscale heterogeneous catalytic hydrogenation.

Further efforts were directed to the development of the concept by employing micro-engineering technologies to produce micro-structured lab-on-a-chip reactors with the catalyst (sputtered Pt) deposited on the inner surface of the channels.[231] It was found that these reactors did not provide PHIP. However, these studies provided a platform for further development of RD NMR for future HP applications, for example, by using Hadamard encoding to achieve a better chemical resolution.[231b]

10.3. Outcome and Perspectives

The current advances and future prospects in RD MRI with HP gases already offer many interesting applications as highlighted above. The major issues concerning the methodology are related to the availability of HP gases and the lifetime of hyperpolarization. HP ^{129}Xe is typically more expensive than the ^{1}H HP hydrocarbon gases produced using PHIP. On the other hand, the nuclear spin relaxation causes more severe problems in the case of HP hydrocarbons. Recent developments in the field of long-lived nuclear spin states,[232] however, may alleviate (or at least mitigate) the latter problem. For instance, it has been shown that a long-lived HP state in ethylene gas can survive for ca. 15 min.[233] The further RD NMR development could concern utilization of such extremely long-lived HP states. In addition, the progress achieved in the field of single-scan ultrafast NMR techniques[234] also offers new capabilities in the context of NMR hyperpolarization. For example, recent work demonstrates the feasibility of single-scan 2D Laplace NMR experiments of dissolved HP propene,[235] and the method should be applicable, e.g., for the investigation of dynamics and physical environments of HP gases in porous media, both with high-field and low-field (mobile) NMR instruments.[235–236]

11. Conclusion

The development and applications of HP gases continue to advance, and show no sign of slowing down. In addition to SEOP hyperpolarization for production of HP ^{3}He and ^{129}Xe, (i) the SEOP HP technique has been expanded to several other noble gases, (ii) the heterogeneous PHIP[28a] technique has enabled production of HP hydrocarbons in pure form (free from contamination by the catalyst), and (iii) the dissolution DNP technique was demonstrated for production of HP ^{129}Xe[26,53a] and $^{15}N_2O$ gases.[237] Thus, many other gases could be potentially amenable to DNP hyperpolarization.

As a result of these fundamental advances in the physics, chemistry and engineering of hyperpolarization processes, which enabled more efficient production of established HP gases (e.g., higher throughput and greater polarization in ^{129}Xe hyperpolarizers)[43i,238] and other advances that enabled the production of new HP gases, it was possible to significantly expand the reach of applications of HP gases in biomedicine and other fields. For example, as described in this mini-review, HP ^{129}Xe is now being employed for in vivo thermometry, brown fat imaging, targeted biosensors, and many other exciting applications, whereas HP hydrocarbons are already used for high-resolution 3D imaging, remote detection, and microfluidic imaging. Many other new applications will likely emerge given that HP gases are becoming more available to researchers, because hyperpolarization equipment is becoming more readily available through commercial sources (as opposed to custom made in the research labs of specialists, as was generally the case only one decade ago). So far, basic and translational scientists have been the main driving force behind the development of MRI of hyperpolarized gases. However, before their entry into routine clinical practice, further research is needed to improve image quality and validate its use, qualitatively and quantitatively, in respiratory disease. This will undoubtedly require collaboration between physicists, chemists and clinicians. Moreover, the better-established applications (e.g., lung imaging using HP ^{129}Xe) will likely continue to be more fully developed, to the point when studies will be driven by medical doctors (the ultimate users of this technology) rather than by the physicists and chemists who pioneered the technology and helped bring it from the proof-of-principle stage to the clinical scale. We look forward to all of these developments with great excitement.

Acknowledgements

The Hyperpolarised Lung Function Imaging Facility (HILF), within the Sir Peter Mansfield Magnetic Imaging Centre (SPMIC) at University of Nottingham, where the M.J.B., S.S. and I.P.H. undertake research into novel functional MRI techniques, is the beneficiary of grants provided by UK's Medical Research Council (MRC) and Engineering and Physical Sciences Research

Council (EPSRC). M.G.S. thanks Burroughs Wellcome Fund Career Award at the Scientific Interface, Human Frontiers Science Program no. RGP0050, and Heritage Medical Research Institute for funding. A.M.C. thanks NIH 1F32EB021840 career award. We thank the following award for funding support: NSF CHE-1416268 and CHE-1416432 (E.Y.C., B.M.G., I.V.K., K.V.K.), NIH 1R21EB018014 and 1R21EB020323 (E.Y.C. and B.M.G.), DOD CDMRP BRP W81XWH-12-1-0159/BC112431 (EYC), PRMRP W81XWH-15-1-0271 and W81XWH-15-1-0272 (E.Y.C., M.S.R., B.M.G.), ExxonMobil Research and Engineering Company Knowledge Build (E.Y.C.). K.V.K., V.V.Z. and I.V.K. thank the Russian Science Foundation (grant 14-35-00020) for support of the MRI experiments. K.V.K. thanks President's of Russian Federation Funding (Grant # MK-4498.2016.3). V.V.T. acknowledges the Academy of Finland (grant numbers 289649 and 294027) for the financial support. Part of this work has been supported by the European Research Council under the European Community's Seventh Framework Programme (FP7/2007–2013)/ERC grant agreement no. 242710 to L.S.) and the Leibniz Association (WGL; grant SAW-2011-FMP-2 to L.S.).

Keywords: gas · hyperpolarization · MRI · NMR · propane · Xe-129

[1] a) P. Nikolaou, A. Coffey, M. Barlow, M. Rosen, B. Goodson, E. Chekmenev, *Anal. Chem.* **2014**, *86*, 8206 – 8212; b) C. Witte, L. Schröder, *NMR Biomed.* **2013**, *26*, 788 – 802; c) J. Ardenkjaer-Larsen, B. Fridlund, A. Gram, G. Hansson, L. Hansson, M. Lerche, R. Servin, M. Thaning, K. Golman, *Proc. Natl. Acad. Sci. USA* **2003**, *100*, 10158 – 10163.

[2] a) B. M. Goodson, N. Whiting, A. M. Coffey, P. Nikolaou, F. Shi, B. Gust, M. E. Gemeinhardt, R. V. Shchepin, J. G. Skinner, J. R. Birchall, M. J. Barlow, E. Y. Chekmenev in *Hyperpolarization Methods for MRS, Vol. 4* (Eds.: J. Griffiths, P. Bottomley, R. E. Wasylishen), Wiley, Chichester, **2015**, pp. 797 – 810; b) P. Nikolaou, B. Goodson, E. Chekmenev, *Chem. Eur. J.* **2015**, *21*, 3156 – 3166; c) B. Goodson, *J. Magn. Reson.* **2002**, *155*, 157 – 216.

[3] M. L. Hirsch, N. Kalechofsky, A. Belzer, M. Rosay, J. G. Kempf, *J. Am. Chem. Soc.* **2015**, *137*, 8428 – 8434.

[4] T. Walker, W. Happer, *Rev. Mod. Phys.* **1997**, *69*, 629.

[5] H. R. Ward, *Acc. Chem. Res.* **1972**, *5*, 18 – 24.

[6] K. H. Mok, P. J. Hore, *Methods* **2004**, *34*, 75 – 87.

[7] a) C. Bowers, D. Weitekamp, *Phys. Rev. Lett.* **1986**, *57*, 2645 – 2648; b) C. Bowers, D. Weitekamp, *J. Am. Chem. Soc.* **1987**, *109*, 5541 – 5542; c) T. Eisenschmid, R. Kirss, P. Deutsch, S. Hommeltoft, R. Eisenberg, J. Bargon, R. Lawler, A. Balch, *J. Am. Chem. Soc.* **1987**, *109*, 8089 – 8091.

[8] R. Adams, J. Aguilar, K. Atkinson, M. Cowley, P. Elliott, S. Duckett, G. Green, I. Khazal, J. Lopez-Serrano, D. Williamson, *Science* **2009**, *323*, 1708 – 1711.

[9] a) I. V. Koptyug, K. V. Kovtunov, S. R. Burt, M. S. Anwar, C. Hilty, S.-I. Han, A. Pines, R. Z. Sagdeev, *J. Am. Chem. Soc.* **2007**, *129*, 5580 – 5586; b) L. S. Bouchard, K. V. Kovtunov, S. R. Burt, M. S. Anwar, I. V. Koptyug, R. Z. Sagdeev, A. Pines, *Angew. Chem. Int. Ed.* **2007**, *46*, 4064 – 4068; *Angew. Chem.* **2007**, *119*, 4142 – 4146.

[10] B. M. Goodson, *J. Magn. Reson.* **2002**, *155*, 157 – 216.

[11] a) T. R. Carver, C. P. Slichter, *Phys. Rev.* **1953**, *92*, 212 – 213; b) A. Overhauser, *Phys. Rev.* **1953**, *92*, 411 – 415; c) J. Natterer, J. Bargon, *Prog. Nucl. Magn. Reson. Spectrosc.* **1997**, *31*, 293 – 315.

[12] K. Golman, O. Axelsson, H. Johannesson, S. Mansson, C. Olofsson, J. Petersson, *Magn. Reson. Med.* **2001**, *46*, 1 – 5.

[13] a) C. Gabellieri, S. Reynolds, A. Lavie, G. S. Payne, M. O. Leach, T. R. Eykyn, *J. Am. Chem. Soc.* **2008**, *130*, 4598 – 4599; b) F. Reineri, A. Viale, S. Ellena, D. Alberti, T. Boi, G. Giovenzana, R. Gobetto, S. Premkumar, S. Aime, *J. Am. Chem. Soc.* **2012**, *134*, 11146 – 11152; c) T. Theis, M. Truong, A. Coffey, E. Chekmenev, W. Warren, *J. Magn. Reson.* **2014**, *248*, 23 – 26; d) T. Theis, M. Truong, A. Coffey, R. Shchepin, K. Waddell, F. Shi, B. Goodson, W. Warren, E. Chekmenev, *J. Am. Chem. Soc.* **2015**, *137*, 1404 – 1407.

[14] M. Plaumann, U. Bommerich, T. Trantzschel, D. Lego, S. Dillenberger, G. Sauer, J. Bargon, G. Buntkowsky, J. Bernarding, *Chem. Eur. J.* **2013**, *19*, 6334 – 6339.

[15] V. V. Zhivonitko, I. V. Skovpin, I. V. Koptyug, *Chem. Commun.* **2015**, *51*, 2506 – 2509.

[16] G. E. Pavlovskaya, Z. I. Cleveland, K. F. Stupic, R. J. Basaraba, T. Meersmann, *Proc. Natl. Acad. Sci. USA* **2005**, *102*, 18275 – 18279.

[17] a) B. Goodson, *Concepts Magn. Reson.* **1999**, *11*, 203 – 223; b) T. Walker, *J. Phys. Conf. Ser.* **2011**, 012001.

[18] D. Lilburn, G. E. Pavlovskaya, T. Meersmann, *J. Magn. Reson.* **2013**, *229*, 173 – 186.

[19] K. Golman, R. in't Zandt, M. Thaning, *Proc. Natl. Acad. Sci. USA* **2006**, *103*, 11270 – 11275.

[20] a) J. Kurhanewicz, D. Vigneron, K. Brindle, E. Chekmenev, A. Comment, C. Cunningham, R. DeBerardinis, G. Green, M. Leach, S. Rajan, R. Rizi, B. Ross, W. Warren, C. Malloy, *Neoplasia* **2011**, *13*, 81 – 97; b) K. M. Brindle, *J. Am. Chem. Soc.* **2015**, *137*, 6418 – 6427; c) A. Comment, M. E. Merritt, *Biochemistry* **2014**, *53*, 7333 – 7357; d) A. Comment, *J. Magn. Reson.* **2016**, *264*, 39 – 48; e) K. R. Keshari, D. M. Wilson, *Chem. Soc. Rev.* **2014**, *43*, 1627 – 1659; f) I. V. Koptyug, *Mendeleev Commun.* **2013**, *23*, 299 – 312; g) S. Meier, P. R. Jensen, M. Karlsson, M. H. Lerche, *Sensors* **2014**, *14*, 1576 – 1597; h) M. H. Lerche, P. R. Jensen, M. Karlsson, S. Meier, *Anal. Chem.* **2015**, *87*, 119 – 132.

[21] a) N. Eshuis, B. van Weerdenburg, M. Feiters, F. Rutjes, S. Wijmenga, M. Tessari, *Angew. Chem. Int. Ed.* **2015**, *54*, 1481 – 1484; *Angew. Chem.* **2015**, *127*, 1501 – 1504; b) C. Hilty, M. Ragavan, *Anal. Chem.* **2015**, *87*, 1004 – 1008.

[22] J. Mugler, T. Altes, *J. Magn. Reson. Imaging* **2013**, *37*, 313 – 331.

[23] R. Branca, T. He, L. Zhang, C. Floyd, M. Freeman, C. White, A. Burant, *Proc. Natl. Acad. Sci. USA* **2014**, *111*, 18001 – 18006.

[24] L. Schröder, *Physica Medica-Eur. J. Med. Phys.* **2013**, *29*, 3 – 16.

[25] M. G. Shapiro, R. M. Ramirez, L. J. Sperling, G. Sun, J. Sun, A. Pines, D. V. Schaffer, V. S. Bajaj, *Nat. Chem.* **2014**, *6*, 629 – 634.

[26] a) A. Comment, S. Jannin, J.-N. Hyacinthe, P. Miéville, R. Sarkar, P. Ahuja, P. R. Vasos, X. Montet, F. Lazeyras, J.-P. Vallée, *Phys. Rev. Lett.* **2010**, *105*, 018104; b) N. Kuzma, M. Pourfathi, H. Kara, P. Manasseh, R. Ghosh, J. Ardenkjaer-Larsen, S. Kadlecek, R. Rizi, *J. Chem. Phys.* **2012**, *137*, 104508.

[27] B. Vuichoud, E. Canet, J. Milani, A. Bornet, D. Baudouin, L. Veyre, D. Gajan, L. Emsley, A. Lesage, C. Copéret, C. Thieuleux, G. Bodenhausen, I. Koptyug, S. Jannin, *J. Phys. Chem. Lett.* **2016**, *7*, 3235 – 3239.

[28] a) L.-S. Bouchard, S. R. Burt, M. S. Anwar, K. V. Kovtunov, I. V. Koptyug, A. Pines, *Science* **2008**, *319*, 442 – 445; b) K. V. Kovtunov, I. E. Beck, V. I. Bukhtiyarov, I. V. Koptyug, *Angew. Chem. Int. Ed.* **2008**, *47*, 1492 – 1495; *Angew. Chem.* **2008**, *120*, 1514 – 1517.

[29] K. Kovtunov, V. Zhivonitko, I. Skovpin, D. Barskiy, I. Koptyug, *Top. Curr. Chem.* **2013**, *338*, 123 – 180.

[30] M. Carravetta, O. G. Johannessen, M. H. Levitt, *Phys. Rev. Lett.* **2004**, *92*, 153003.

[31] J. Brossel, A. Kastler, *C. R. Acad. Sci.* **1949**, *229*, 1213 – 1215.

[32] M. R. Bouchiat, T. R. Carver, C. M. Varnum, *Phys. Rev. Lett.* **1960**, *5*, 373 – 375.

[33] B. C. Grover, *Phys. Rev. Lett.* **1978**, *40*, 391.

[34] a) W. Happer, E. Miron, S. Schaefer, D. Schreiber, W. V. Wijngaarden, X. Zeng, *Phys. Rev. A* **1984**, *29*, 3092 – 3110; b) G. D. Cates, R. J. Fitzgerald, A. S. Barton, P. Bogorad, M. Gatzke, N. R. Newbury, B. Saam, *Phys. Rev. A* **1992**, *45*, 4631 – 4639; c) T. E. Chupp, M. E. Wagshul, K. P. Coulter, A. B. Mcdonald, W. Happer, *Phys. Rev. C* **1987**, *36*, 2244 – 2251.

[35] T. Meersmann, E. Brunner in *Hyperpolarized Xenon-129 Magnetic Resonance: Concepts, Production, Techniques and Applications*, RSC, Cambridge, **2015**.

[36] a) T. E. Chupp, K. P. Coulter, *Phys. Rev. Lett.* **1985**, *55*, 1074; b) R. Stoner, R. Walsworth, *Phys. Rev. A* **2002**, *66*, 032704.

[37] Ref. [16].

[38] K. F. Stupic, Z. I. Cleveland, G. E. Pavlovskaya, T. Meersmann, *J. Magn. Reson.* **2011**, *208*, 58 – 69.

[39] D. Steck in Rubidium 85 D line data, Rubidium 87 D line data (revision 2.1.5, 13 January 2015), Vol.

[40] a) E. Babcock, B. Chann, I. A. Nelson, T. G. Walker, *Appl. Opt.* **2005**, *44*, 3098 – 3104; b) N. Whiting, P. Nikolaou, N. Eschmann, M. Barlow, R. Lammert, J. Ungar, W. Hu, L. Vaissie, B. Goodson, *Appl. Phys. B* **2012**, *106*, 775 – 788.

[41] E. Babcock, I. Nelson, S. Kadlecek, B. Driehuys, L. W. Anderson, F. W. Hersman, T. G. Walker, *Phys. Rev. Lett.* **2003**, *91*, 123003.

[42] a) X. Z. Zeng, C. J. Wu, M. X. Zhao, S. L. Li, L. Y. Li, X. T. Zhang, Z. D. Liu, W. Y. Liu, *Chem. Phys. Lett.* **1991**, *182*, 538 – 540; b) N. Whiting, N. A. Eschmann, B. M. Goodson, M. J. Barlow, *Phys. Rev. A* **2011**, *83*, 053428.

[43] a) D. Raftery, H. Long, T. Meersmann, P. J. Grandinetti, L. Reven, A. Pines, *Phys. Rev. Lett.* **1991**, *66*, 584 – 587; b) M. S. Rosen, T. E. Chupp, K. P. Coulter, R. C. Welsh, S. D. Swanson, *Rev. Sci. Instrum.* **1999**, *70*, 1546; c) U. Ruth, T. Hof, J. Schmidt, D. Fick, H. J. Jänsch, *Appl. Phys. B* **1999**, *68*, 93 – 97; d) H. Desvaux, T. Gautier, G. Le Goff, M. Pétro, P. Berthault, *Eur. Phys. J. B* **2000**, *12*, 289 – 296; e) P. Nikolaou, N. Whiting, N. A. Eschmann, K. E. Chaffee, B. M. Goodson, *J. Magn. Reson.* **2009**, *197*, 249 – 254; f) S. R. Parnell, M. H. Deppe, J. Parra-Robles, J. M. Wild, *J. Appl. Phys.* **2010**, *108*, 064908; g) N. Whiting, P. Nikolaou, N. A. Eschmann, B. M. Goodson, M. J. Barlow, *J. Magn. Reson.* **2011**, *208*, 298 – 304; h) J. S. Six, T. Hughes-Riley, K. F. Stupic, G. E. Pavlovskaya, T. Meersmann, *PLoS One* **2012**, *7*, e49927; i) P. Nikolaou, A. Coffey, L. Walkup, B. Gust, N. Whiting, H. Newton, S. Barcus, I. Muradyan, M. Dabaghyan, G. Moroz, M. Rosen, S. Patz, M. Barlow, E. Chekmenev, B. Goodson, *Proc. Natl. Acad. Sci. USA* **2013**, *110*, 14150 – 14155; j) T. Hughes-Riley, J. S. Six, D. M. Lilburn, K. F. Stupic, A. C. Dorkes, D. E. Shaw, G. E. Pavlovskaya, T. Meersmann, *J. Magn. Reson.* **2013**, *237*, 23 – 33; k) P. Nikolaou, A. M. Coffey, L. L. Walkup, B. M. Gust, N. R. Whiting, H. Newton, I. Muradyan, M. Dabaghyan, K. Ranta, G. Moroz, S. Patz, M. S. Rosen, M. J. Barlow, E. Y. Chekmenev, B. M. Goodson, *Magn. Reson. Imaging* **2014**, *32*, 541 – 550; l) P. Nikolaou, A. M. Coffey, L. L. Walkup, B. Gust, C. LaPierre, E. Koehnemann, M. J. Barlow, M. S. Rosen, B. M. Goodson, E. Y. Chekmenev, *J. Am. Chem. Soc.* **2014**, *136*, 1636 – 1642; m) P. Nikolaou, A. M. Coffey, K. Ranta, L. L. Walkup, B. Gust, M. J. Barlow, M. S. Rosen, B. M. Goodson, E. Y. Chekmenev, *J. Phys. Chem. B* **2014**, *118*, 4809 – 4816.

[44] a) B. Driehuys, G. Cates, E. Miron, K. Sauer, D. Walter, W. Happer, *Appl. Phys. Lett.* **1996**, *69*, 1668 – 1670; b) M. Haake, A. Pines, J. A. Reimer, R. Seydoux, *J. Am. Chem. Soc.* **1997**, *119*, 11711 – 11712; c) A. L. Zook, B. B. Adhyaru, C. R. Bowers, *J. Magn. Reson.* **2002**, *159*, 175 – 182; d) M. G. Mortuza, S. Anala, G. E. Pavlovskaya, T. J. Dieken, T. Meersmann, *J. Chem. Phys.* **2003**, *118*, 1581; e) K. Knagge, J. Prange, D. Raftery, *Chem. Phys. Lett.* **2004**, *397*, 11 – 16; f) I. C. Ruset, S. Ketel, F. W. Hersman, *Phys. Rev. Lett.* **2006**, *96*, 053002; g) G. Schrank, Z. Ma, A. Schoeck, B. Saam, *Phys. Rev. A* **2009**, *80*, 063424; h) G. Norquay, S. R. Parnell, X. Xu, J. Parra-Robles, J. M. Wild, *J. Appl. Phys.* **2013**, *113*, 044908; i) A. Nossov, E. Haddad, F. Guenneaua, A. Gédéon, *Phys. Chem. Chem. Phys.* **2003**, *5*, 4473 – 4478.

[45] a) K. F. Stupic, Z. I. Cleveland, G. E. Pavlovskaya, T. Meersmann, *Solid State Nucl. Magn. Reson.* **2006**, *29*, 79 – 84; b) Z. Wu, W. Happer, M. Kitano, J. Daniels, *Phys. Rev. A* **1990**, *42*, 2774; c) R. K. Ghosh in *Spin Exchange Optical Pumping of Neon and its Applications*, Princeton University, Princeton, **2009**; d) S. Fain, M. L. Schiebler, D. G. McCormack, G. Parraga, *J. Magn. Reson. Imaging* **2010**, *32*, 1398 – 1408.

[46] G. D. Cates, D. R. Benton, M. Gatzke, W. Happer, K. C. Hasson, N. R. Newbury, *Phys. Rev. Lett.* **1990**, *65*, 2591 – 2594.

[47] a) B. Chann, I. Nelson, T. G. Walker, *Opt. Lett.* **2000**, *25*, 1352 – 1354; b) J. N. Zerger, M. J. Lim, K. P. Coulter, T. E. Chupp, *Appl. Phys. Lett.* **2000**, *76*, 1798 – 1800.

[48] F. D. Colegrove, L. D. Scheare, G. K. Walters, *Phys. Rev.* **1963**, *132*, 2561 – 2572.

[49] a) T. R. Gentile, D. R. Rich, A. K. Thompson, W. M. Snow, G. L. Jones, *J. Res. Natl. Inst. Stand. Technol.* **2001**, *106*, 709 – 729; b) P. J. Nacher, G. Tastevin, X. Maitre, X. Dollat, B. Lemaire, J. Olejnik, *Eur. J. Radiol.* **1999**, *9*, b18.

[50] M. Ebert, T. Grossmann, W. Heil, W. E. Otten, R. Surkau, M. Leduc, P. Bachert, M. V. Knopp, L. R. Schad, M. Thelen, *Lancet* **1996**, *11*, 9011.

[51] a) L. D. Schearer, *Phys. Rev.* **1969**, *180*, 83 – 90; b) L. Young, D. Yang, R. W. Dunford, *J. Phys. B* **2002**, *35*, 2985 – 2992; c) T. Hadeishi, L. Chung-Heng, *Phys. Rev. Lett.* **1967**, *19*, 211; d) V. Lefevre-Seguin, M. Leduc, *J. Phys. B* **1977**, *10*, 2157.

[52] a) G. Frossati, *J. Low Temp. Phys.* **1998**, *111*, 521 – 532; b) M. Tanaka, T. Kunimatsu, M. Fujiwara, H. Kohri, T. Ohta, M. Utsuro, M. Yosoi, S. Ono, K. Fukuda, K. Takamatsu, K. Ueda, J.-P. Didelez, G. Frossati, A. D. Waard, *J. Phys. Conf. Ser.* **2011**, *295*, 012167; c) J. D. O'Neill, E. V. Krjukov, J. R. Owers-Bradley, Y. Xia, *J. Low Temp. Phys.* **2007**, *146*, 563 – 579; d) E. V. Krjukov, J. D. O'Neill, J. R. Owers-Bradley, *J. Low Temp. Phys.* **2005**, *140*, 397 – 408.

[53] a) M. Pourfathi, N. N. Kuzma, H. Kara, R. K. Ghosh, H. Shaghaghi, S. J. Kadlecek, R. R. Rizi, *J. Magn. Reson.* **2013**, *235*, 71 – 76; b) A. Capozzi, C. Roussel, A. Comment, J. N. Hyacinthe, *J. Phys. Chem. C* **2015**, *119*, 5020 – 5025; c) A. Capozzi, J. N. Hyacinthe, T. Cheng, T. R. Eichhorn, G. Boero, C. Roussel, J. J. van der Klink, A. Comment, *J. Phys. Chem. C* **2015**, *119*, 22632 – 22639.

[54] J. H. Ardenkjaer-Larsen, A. M. Leach, N. Clarke, J. Urbahn, D. Anderson, T. W. Skloss, *NMR Biomed.* **2011**, *24*, 927 – 932.

[55] a) T. E. Chupp, R. J. Hoare, R. L. Walsworth, B. Wu, *Phys. Rev. Lett.* **1994**, *72*, 2363; b) N. R. Newbury, A. S. Barton, P. Bogorad, G. D. Cates, M. Gatzke, B. Saam, L. Han, R. Holmes, P. A. Souder, J. Xu, D. Benton, *Phys. Rev. Lett.* **1991**, *67*, 3219.

[56] a) A. K. Thompson, A. M. Bernstein, T. E. Chupp, D. J. DeAngelis, G. E. Dodge, G. Dodson, K. A. Dow, M. Farkhondeh, W. Fong, J. Y. Kim, R. A. Loveman, J. M. Richardson, H. Schmieden, D. R. Tieger, T. C. Yates, M. E. Wagshul, J. D. Zumbro, *Phys. Rev. Lett.* **1992**, *68*, 2901; b) J. T. Singh, P. A. M. Dolph, W. A. Tobias, T. D. Averett, A. Kelleher, K. E. Mooney, V. V. Nelyubin, Y. Wang, Y. Zheng, G. D. Cates, *Phys. Rev. C* **2015**, *91*, 055205; c) E. Lelievre-Berna, *Phys. B* **2007**, *397*, 162 – 167; d) T. R. Gentile, W. C. Chen, *Proc. Sci. (PSTP)* **2013**, *022*, 1 – 11; e) S. Karpuk, F. Allmendinger, M. Burghoff, C. Gemmel, M. Güldner, W. Heil, W. Kilian, S. Knappe-Grüneberg, C. Mrozik, W. Müller, E. W. Otten, M. Repetto, Z. Salhi, U. Schmidt, A. Schnabel, F. Seifert, Y. Sobolev, L. Trahms, K. Tullney, *Phys. Part. Nucl.* **2013**, *44*, 904 – 908.

[57] a) D. Raftery, L. Reven, H. Long, A. Pines, P. Tang, J. A. Reimer, *J. Phys. Chem.* **1993**, *97*, 1649 – 1655; b) C. R. Bowers, T. Pietrass, E. Barash, A. Pines, R. K. Grubbs, A. P. Alivisatos, *J. Phys. Chem.* **1994**, *98*, 9400 – 9404; c) T. Pietrass, A. Bifone, A. Pines, *Surf. Sci.* **1995**, *334*, L730 – L734.

[58] a) C. R. Bowers, H. W. Long, T. Pietrass, H. C. Gaede, A. Pines, *Chem. Phys. Lett.* **1993**, *205*, 168 – 170; b) B. Driehuys, G. D. Cates, W. Happer, H. Mabuchi, B. Saam, M. S. Albert, A. Wishnia, *Phys. Lett. A* **1993**, *184*, 88 – 92; c) H. W. Long, H. C. Gaede, J. Shore, L. Reven, C. R. Bowers, J. Kritzenberger, T. Pietrass, A. Pines, P. Tang, J. A. Reimer, *J. Am. Chem. Soc.* **1993**, *115*, 8491 – 8492; d) B. Driehuys, G. D. Cates, W. Happer, *Phys. Rev. Lett.* **1995**, *74*, 4943 – 4946; e) H. C. Gaede, Y. Q. Song, R. E. Taylor, E. J. Munson, J. A. Reimer, A. Pines, *Appl. Magn. Reson.* **1995**, *8*, 373 – 384; f) T. Room, S. Appelt, R. Seydoux, E. L. Hahn, A. Pines, *Phys. Rev. B* **1997**, *55*, 11604 – 11610; g) G. Navon, Y. Q. Song, T. Room, S. Appelt, R. E. Taylor, A. Pines, *Science* **1996**, *271*, 1848 – 1851; h) R. J. Fitzgerald, K. L. Sauer, W. Happer, *Chem. Phys. Lett.* **1998**, *284*, 87 – 92; i) T. Pietrass, R. Seydoux, A. Pines, *J. Magn. Reson.* **1998**, *133*, 299 – 303; j) S. Appelt, F. Haesing, S. Baer-Lang, N. Shah, B. Blumich, *Chem. Phys. Lett.* **2001**, *348*, 263 – 269.

[59] a) M. Haake, A. Pines, J. A. Reimer, R. Seydoux, *J. Am. Chem. Soc.* **1997**, *119*, 11711 – 11712; b) R. Seydoux, A. Pines, M. Haake, J. A. Reimer, *J. Phys. Chem. B* **1999**, *103*, 4629 – 4637; c) ref. [44b].

[60] a) D. Raftery, E. MacNamara, G. Fisher, C. V. Rice, J. Smith, *J. Am. Chem. Soc.* **1997**, *119*, 8746 – 8747; b) E. Brunner, M. Haake, A. Pines, J. A. Reimer, R. Seydoux, *Chem. Phys. Lett.* **1998**, *290*, 112 – 116; c) E. Brunner, R. Seydoux, M. Haake, A. Pines, J. A. Reimer, *J. Magn. Reson.* **1998**, *130*, 145 – 148; d) E. MacNamara, G. Fisher, J. Smith, C. V. Rice, S. J. Hwang, D. Raftery, *J. Phys. Chem. B* **1999**, *103*, 1158 – 1160.

[61] a) B. Saam, N. Drukker, W. Happer, *Chem. Phys. Lett.* **1996**, *263*, 481 – 487; b) D. M. Schmidt, J. S. George, S. I. Penttila, A. Caprihan, E. Fukushima, *J. Magn. Reson.* **1997**, *129*, 184 – 187; c) Y. Song, B. Goodson, B. Sheridan, T. de Swiet, A. Pines, *J. Chem. Phys.* **1998**, *108*, 6233 – 6239.

[62] a) R. W. Mair, D. G. Cory, S. Peled, C. H. Tseng, S. Patz, R. L. Walsworth, *J. Magn. Reson.* **1998**, *135*, 478 – 486; b) R. W. Mair, G. P. Wong, D. Hoffmann, M. D. Hurlimann, S. Patz, L. M. Schwartz, R. L. Walsworth, *Phys. Rev. Lett.* **1999**, *83*, 3324 – 3327; c) S. Peled, C. H. Tseng, A. A. Sodickson, R. W. Mair, R. L. Walsworth, D. G. Cory, *J. Magn. Reson.* **1999**, *140*, 320 – 324.

[63] a) I. L. Moudrakovski, A. Sanchez, C. I. Ratcliffe, J. A. Ripmeester, *J. Phys. Chem. B* **2000**, *104*, 7306 – 7310; b) G. P. Wong, R. W. Mair, R. L. Walsworth, D. G. Cory, *Phys. Rev. Lett.* **2001**, *86*, 4156 – 4159.

[64] a) E. Brunner, M. Haake, L. Kaiser, A. Pines, J. A. Reimer, *J. Magn. Reson.* **1999**, *138*, 155 – 159; b) L. G. Kaiser, T. Meersmann, J. W. Logan, A. Pines, *Proc. Natl. Acad. Sci. USA* **2000**, *97*, 2414 – 2418.

[65] a) I. L. Moudrakovski, S. Lang, C. I. Ratcliffe, B. Simard, G. Santyr, J. A. Ripmeester, *J. Magn. Reson.* **2000**, *144*, 372 – 377; b) G. Pavlovskaya, J. Six, T. Meersman, N. Gopinathan, S. P. Rigby, *AIChE J.* **2015**, *61*, 4013 – 4019.

[66] a) H. J. Jänsch, T. Hof, U. Ruth, J. Schmidt, D. Stahl, D. Fick, *Chem. Phys. Lett.* **1998**, *296*, 146 – 150; b) H. J. Jansch, P. Gerhard, M. Koch, *Proc. Natl. Acad. Sci. USA* **2004**, *101*, 13715 – 13719.

[67] a) X. X. Li, C. Newberry, I. Saha, P. Nikolaou, N. Whiting, B. M. Goodson, *Chem. Phys. Lett.* **2006**, *419*, 233 – 239; b) A. E. Truxal, C. C. Slack, M. D. Gomes, C. C. Vassiliou, D. E. Wemmer, A. Pines, *Angew. Chem. Int. Ed.* **2016**, *55*, 4666; *Angew. Chem.* **2016**, *128*, 4744.

[68] a) S. Anala, G. E. Pavlovskaya, P. Pichumani, T. J. Dieken, M. D. Olsen, T. Meersmann, *J. Am. Chem. Soc.* **2003**, *125*, 13298 – 13302; b) N. J. Rogers, F. Hill-Casey, K. F. Stupic, J. S. Six, C. Lesbats, S. P. Rigby, J. Fraissard, G. E. Pavlovskaya, T. Meersmann, *Proc. Natl. Acad. Sci. USA* **2016**, *113*, 3164 – 3168.

[69] a) T. Meersmann, J. W. Logan, R. Simonutti, S. Caldarelli, A. Comotti, P. Sozzani, L. G. Kaiser, A. Pines, *J. Phys. Chem. A* **2000**, *104*, 11665 – 11670; b) P. Sozzani, A. Comotti, R. Simonutti, T. Meersmann, J. W. Logan, A. Pines, *Angew. Chem. Int. Ed.* **2000**, *39*, 2695 – 2698; *Angew. Chem.* **2000**, *112*, 2807 – 2810; c) I. Moudrakovski, D. V. Soldatov, J. A. Ripmeester, D. N. Sears, C. J. Jameson, *Proc. Natl. Acad. Sci. USA* **2004**, *101*, 17924 – 17929; d) D. V. Soldatov, I. L. Moudrakovski, E. V. Grachev, J. A. Ripmeester, *J. Am. Chem. Soc.* **2006**, *128*, 6737 – 6744; e) C. Y. Cheng, C. R. Bowers, *J. Am. Chem. Soc.* **2007**, *129*, 13997 – 14002; f) C. Y. Cheng, C. R. Bowers, *ChemPhysChem* **2007**, *8*, 2077 – 2081; g) C. Y. Cheng, T. C. Stamatatos, G. Christou, C. R. Bowers, *J. Am. Chem. Soc.* **2010**, *132*, 5387 – 5393; h) C. R. Bowers, M. Dvoyashkin, S. R. Salpage, C. Akel, H. Bhase, M. F. Geer, L. S. Shimizu, *ACS Nano* **2015**, *9*, 6343 – 6353; i) R. Anedda, D. V. Soldatov, I. L. Moudrakovski, M. Casu, J. A. Ripmeester, *Chem. Mater.* **2008**, *20*, 2908 – 2920.

[70] A. Comotti, S. Bracco, L. Ferretti, M. Mauri, R. Simonutti, P. Sozzani, *Chem. Commun.* **2007**, 350 – 352.

[71] J. M. Kneller, R. J. Soto, S. E. Surber, J. F. Colomer, A. Fonseca, J. B. Nagy, G. Van Tendeloo, T. Pietrass, *J. Am. Chem. Soc.* **2000**, *122*, 10591 – 10597.

[72] I. L. Moudrakovski, A. A. Sanchez, C. I. Ratcliffe, J. A. Ripmeester, *J. Phys. Chem. B* **2001**, *105*, 12338 – 12347.

[73] a) A. V. Nossov, D. V. Soldatov, J. A. Ripmeester, *J. Am. Chem. Soc.* **2001**, *123*, 3563 – 3568; b) J. P. Butler, R. W. Mair, D. Hoffmann, M. I. Hrovat, R. A. Rogers, G. P. Topulos, R. L. Walsworth, S. Patz, *J. Phys. Condens. Matter* **2002**, *14*, L297 – L304; c) I. L. Moudrakovski, L. Q. Wang, T. Baumann, J. H. Satcher, G. J. Exarhos, C. I. Ratcliffe, J. A. Ripmeester, *J. Am. Chem. Soc.* **2004**, *126*, 5052 – 5053; d) I. L. Moudrakovski, C. I. Ratcliffe, J. A. Ripmeester, L. Q. Wang, G. J. Exarhos, T. F. Baumann, J. H. Satcher, *J. Phys. Chem. B* **2005**, *109*, 11215 – 11222; e) R. Simonutti, S. Bracco, A. Comotti, M. Mauri, P. Sozzani, *Chem. Mater.* **2006**, *18*, 4651 – 4657; f) A. Comotti, S. Bracco, P. Sozzani, S. Horike, R. Matsuda, J. Chen, M. Takata, Y. Kubota, S. Kitagawa, *J. Am. Chem. Soc.* **2008**, *130*, 13664 – 13672.

[74] a) K. Campbell, K. J. Ooms, R. E. Wasylishen, R. R. Tykwinski, *Org. Lett.* **2005**, *7*, 3397 – 3400; b) K. J. Ooms, R. E. Wasylishen, *Microporous Mesoporous Mater.* **2007**, *103*, 341 – 351; c) S. Pawsey, I. Moudrakovski, J. Ripmeester, L. Q. Wang, G. J. Exarhos, J. L. C. Rowsell, O. M. Yaghi, *J. Phys. Chem. C* **2007**, *111*, 6060 – 6067.

[75] a) A. Dubes, I. L. Moudrakovski, P. Shahgaldian, A. W. Coleman, C. I. Ratcliffe, J. A. Ripmeester, *J. Am. Chem. Soc.* **2004**, *126*, 6236 – 6237; b) G. S. Ananchenko, I. L. Moudrakovski, A. W. Coleman, J. A. Ripmeester, *Angew. Chem. Int. Ed.* **2008**, *47*, 5616 – 5618; *Angew. Chem.* **2008**, *120*, 5698 – 5700.

[76] P. Sozzani, S. Bracco, A. Comotti, M. Mauri, R. Simonutti, P. Valsesia, *Chem. Commun.* **2006**, 1921 – 1923.

[77] a) A. Nossov, E. Haddad, F. Guenneau, C. Mignon, A. Gedeon, D. Grosso, F. Babonneau, C. Bonhomme, C. Sanchez, *Chem. Commun.* **2002**, 2476 – 2477; b) V. V. Terskikh, I. L. Moudrakovski, S. R. Breeze, S. Lang, C. I. Ratcliffe, J. A. Ripmeester, A. Sayari, *Langmuir* **2002**, *18*, 5653 – 5656; c) A. Nossov, E. Haddad, F. Guenneau, A. Galarneau, F. Di Renzo, F. Fajula, A. Gedeon, *J. Phys. Chem. B* **2003**, *107*, 12456 – 12460; d) A. Comotti, S. Bracco, P. Valsesia, L. Ferretti, P. Sozzani, *J. Am. Chem. Soc.* **2007**, *129*, 8566 – 8576; e) A. Galarneau, M. Nader, F. Guenneau, F. Di Renzo, A. Gedeon, *J. Phys. Chem. C* **2007**, *111*, 8268 – 8277.

[78] a) A. Nossov, F. Guenneau, M. A. Springuel-Huet, E. Haddad, V. Montouillout, B. Knott, F. Engelke, C. Fernandez, A. Gedeon, *Phys. Chem. Chem. Phys.* **2003**, *5*, 4479 – 4483; b) A. Sakthivel, S. J. Huang, W. H. Chen, Z. H. Lan, K. H. Chen, T. W. Kim, R. Ryoo, A. S. T. Chiang, S. B. Liu, *Chem. Mater.* **2004**, *16*, 3168 – 3175; c) A. Sakthivel, S. J. Huang, W. H. Chen, Z. H. Lan, K. H. Chen, H. P. Lin, C. Y. Mou, S. B. Liu, *Adv. Funct. Mater.* **2005**, *15*, 253 – 258; d) Y. Liu, W. P. Zhang, Z. C. Liu, S. T. Xu, Y. D. Wang, Z. K. Xie, X. W. Han, X. H. Bao, *J. Phys. Chem. C* **2008**, *112*, 15375 – 15381; e) Y. Liu, W. P. Zhang, S. J. Xie, L. Xu, X. W. Han, X. H. Bao, *J. Phys. Chem. B* **2008**, *112*, 1226 – 1231; f) L. Itani, Y. Liu, W. P. Zhang, K. N. Bozhilov, L. Delmotte, V. Valtchev, *J. Am. Chem. Soc.* **2009**, *131*, 10127 – 10139; g) H. C. Xin, J. Zhao, S. T. Xu, J. P. Li, W. P. Zhang, X. W. Guo, E. J. M. Hensen, Q. H. Yang, C. Li, *J. Phys. Chem. C* **2010**, *114*, 6553 – 6559; h) K. K. Zhu, J. M. Sun, J. Liu, L. Q. Wang, H. Y. Wan, J. Z. Hu, Y. Wang, C. H. F. Peden, Z. M. Nie, *ACS Catal.* **2011**, *1*, 682 – 690; i) C. Z. Jin, G. Li, X. S. Wang, L. X. Zhao, L. P. Liu, H. O. Liu, Y. Liu, W. P. Zhang, X. W. Han, X. H. Bao, *Chem. Mater.* **2007**, *19*, 1664 – 1670; j) X. J. Li, W. P. Zhang, S. L. Liu, L. Y. Xu, X. W. Han, X. H. Bao, *J. Catal.* **2007**, *250*, 55 – 66.

[79] a) C. J. Jameson, *J. Chem. Phys.* **2002**, *116*, 8912 – 8929; b) C. J. Jameson, A. C. de Dios, *J. Chem. Phys.* **2002**, *116*, 3805 – 3821.

[80] E. Weiland, M. A. Springuel-Huet, A. Nossov, A. Gédéon, *Microporous Mesoporous Mater.* **2016**, *225*, 41 – 65.

[81] J. C. Woods in Congressional Hearing: "Caught by Surprise: Causes and Consequences of the Helium-3 Supply Crisis", Vol. **2010**.

[82] a) J. S. Six, T. Hughes-Riley, D. M. Lilburn, A. C. Dorkes, K. F. Stupic, D. E. Shaw, P. G. Morris, I. P. Hall, G. E. Pavlovskaya, T. Meersmann, *Magn. Reson. Imaging* **2014**, *32*, 48 – 53; b) Z. I. Cleveland, K. F. Stupic, G. E. Pavlovskaya, J. E. Repine, J. B. Wooten, T. Meersmann, *J. Am. Chem. Soc.* **2007**, *129*, 1784 – 1792.

[83] W. Ramsay, *Nobel Lecture*, *Dec* **1904**, *12*, 1901 – 1921.

[84] T. Marx, M. Schmidt, U. Schirmer, H. Reinelt, *J. R. Soc. Med.* **2000**, *93*, 513 – 517.

[85] J. Lawrence, W. Loomis, C. Tobias, F. Turpin, *J. Physiol.* **1946**, *105*, 197.

[86] S. C. Cullen, E. G. Gross, *Science* **1951**, *113*, 580 – 582.

[87] M. Albert, G. Cates, B. Driehuys, W. Happer, B. Saam, C. Springer, A. Wishnia, *Nature* **1994**, *370*, 199 – 201.

[88] a) R. Edelman, H. Hatabu, E. Tadamura, W. Li, P. Prasad, *Nat. Med.* **1996**, *2*, 1236 – 1239; b) H. Kauczor, K. Kreitner, *Eur. Radiol.* **1999**, *9*, 1755 – 1764.

[89] J. Mugler, B. Driehuys, J. Brookeman, G. Cates, S. Berr, R. Bryant, T. Daniel, E. deLange, J. Downs, C. Erickson, W. Happer, D. Hinton, N. Kassel, T. Maier, C. Phillips, B. Saam, K. Sauer, M. Wagshul, *Magn. Reson. Med.* **1997**, *37*, 809 – 815.

[90] L. Zhao, M. Albert, *Nucl. Instrum. Methods Phys. Res. Sect. A* **1998**, *402*, 454 – 460.

[91] a) H. Middleton, R. Black, B. Saam, G. Cates, G. Cofer, R. Guenther, W. Happer, L. Hedlund, G. Johnson, K. Juvan, J. Swartz, *Magn. Reson. Med.* **1995**, *33*, 271 – 275; b) L. Walkup, J. Woods, *NMR Biomed.* **2014**, *27*, 1429 – 1438.

[92] a) Y. Shukla, A. Wheatley, M. Kirby, S. Svenningsen, A. Farag, G. Santyr, N. Paterson, D. McCormack, G. Parraga, *Acad. Radiol.* **2012**, *19*, 941 – 951; b) S. Svenningsen, M. Kirby, D. Starr, D. Leary, A. Wheatley, G. N. Maksym, D. G. McCormack, G. Parraga, *J. Magn. Reson. Imaging* **2013**, *38*, 1521 – 1530.

[93] a) S. S. Kaushik, Z. I. Cleveland, G. P. Cofer, G. Metz, D. Beaver, J. Nouls, M. Kraft, W. Auffermann, J. Wolber, H. P. McAdams, *Magn. Reson. Med.* **2011**, *65*, 1154 – 1165; b) B. Driehuys, S. Martinez-Jimenez, Z. Cleveland, G. Metz, D. Beaver, J. Nouls, S. Kaushik, R. Firszt, C. Willis, K. Kelly, J. Wolber, M. Kraft, H. McAdams, *Radiology* **2012**, *262*, 279 – 289; c) M. Kirby, S. Svenningsen, A. Owrangi, A. Wheatley, A. Farag, A. Ouriadov, G. Santyr, R. Etemad-Rezai, H. Coxson, D. McCormack, G. Parraga, *Radiology* **2012**, *265*, 600 – 610; d) M. Kirby, S. Svenningsen, N. Kanhere, A. Owrangi, A. Wheatley, H. Coxson, G. Santyr, N. Paterson, D. McCormack, G. Parraga, *J. Appl. Physiol.* **2013**, *114*, 707 – 715.

[94] a) S. Kaushik, M. Freeman, S. Yoon, M. Liljeroth, J. Stiles, J. Roos, W. Foster, C. Rackley, H. McAdams, B. Driehuys, *J. Appl. Physiol.* **2014**, *117*, 577 – 585; b) N. J. Stewart, G. Leung, G. Norquay, H. Marshall, J. Parra-Robles, P. S. Murphy, R. F. Schulte, C. Elliot, R. Condliffe, P. D. Griffiths, *Magn. Reson. Med.* **2015**, *74*, 196 – 207.

[95] S. Kaushik, Z. Cleveland, G. Cofer, G. Metz, D. Beaver, J. Nouls, M. Kraft, W. Auffermann, J. Wolber, H. McAdams, B. Driehuys, *Magn. Reson. Med.* **2011**, *65*, 1154 – 1165.

[96] M. Kirby, G. Parraga, *Acad. Radiol.* **2013**, *20*, 1344 – 1356.

[97] B. G. Zeiher, T. J. Gross, J. A. Kern, L. A. Lanza, M. W. Peterson, *Chest* **1995**, *108*, 68 – 72.

[98] a) K. Ruppert, J. Brookeman, K. Hagspiel, J. Mugler, *Magn. Reson. Med.* **2000**, *44*, 349 – 357; b) J. Butler, R. Mair, D. Hoffmann, M. Hrovat, R. Rogers, G. Topulos, R. Walsworth, S. Patz, *J. Phys. Condens. Matter* **2002**, *14*, L297; c) ref. [73b].

[99] K. Qing, K. Ruppert, Y. Jiang, J. Mata, W. Miller, Y. Shim, C. Wang, I. Ruset, F. Hersman, T. Altes, J. Mugler, *J. Magn. Reson. Imaging* **2014**, *39*, 346 – 359.

[100] Z. Cleveland, G. Cofer, G. Metz, D. Beaver, J. Nouls, S. Kaushik, M. Kraft, J. Wolber, K. Kelly, H. McAdams, B. Driehuys, *PLoS One* **2010**, *5*, e12192.

[101] a) J. Mugler, T. Altes, I. Ruset, I. Dregely, J. Mata, G. Miller, S. Ketel, J. Ketel, F. Hersman, K. Ruppert, *Proc. Natl. Acad. Sci. USA* **2010**, *107*, 21707 – 21712; b) Y. V. Chang, J. D. Quirk, I. C. Ruset, J. J. Atkinson, F. W. Hersman, J. C. Woods, *Magn. Reson. Med.* **2014**, *71*, 339 – 344; c) K. Ruppert, J. Mata, J. Brookeman, K. Hagspiel, J. Mugler, *Magn. Reson. Med.* **2004**, *51*, 676 – 687; d) K. Ruppert, J. Mata, H. Wang, W. Tobias, G. Cates, J. Brookeman, K. Hagspiel, J. Mugler, *Magn. Reson. Med.* **2007**, *57*, 1099 – 1109; e) Y. Chang, J. Mata, T. Altes, J. Mugler III, K. Ruppert, *Proceedings of the Joint Annual Meeting of ISMRM-ESMRMB*, Stockholm, Sweden **2010**, p. 4602.

[102] a) Y. V. Chang, *Magn. Reson. Med.* **2013**, *69*, 884 – 890; b) I. Dregely, I. Ruset, J. Mata, J. Ketel, S. Ketel, J. Distelbrink, T. Altes, J. Mugler, G. Miller, F. Hersman, K. Ruppert, *Magn. Reson. Med.* **2012**, *67*, 943 – 953; c) I. Dregely, J. Mugler, I. Ruset, T. Altes, J. Mata, G. Miller, J. Ketel, S. Ketel, J. Distelbrink, F. Hersman, K. Ruppert, *J. Magn. Reson. Imaging* **2011**, *33*, 1052 – 1062.

[103] R. Chen, F.-C. Fan, S. Kim, K. Jan, S. Usami, S. Chien, *J. Appl. Physiol.* **1980**, *49*, 178 – 183.

[104] D. Gur, W. F. Good, S. K. Wolfson, H. Yonas, L. Shabason, *Science* **1982**, *215*, 1267 – 1268.

[105] S. D. Swanson, M. S. Rosen, B. W. Agranoff, K. P. Coulter, R. C. Welsh, T. E. Chupp, *Magn. Reson. Med.* **1997**, *38*, 695 – 698.

[106] a) A. Wakai, K. Nakamura, J. Kershaw, Y. Kondoh, D. Wright, I. Kanno, *Magn. Reson. Med. Sci.* **2005**, *4*, 19 – 25; b) X. Zhou, M. Mazzanti, J. Chen, Y. S. Tzeng, J. Mansour, J. Gereige, A. Venkatesh, Y. Sun, R. Mulkern, M. Albert, *NMR Biomed.* **2008**, *21*, 217 – 225.

[107] G. Duhamel, P. Choquet, J.-L. Leviel, J. Steibel, L. Lamalle, C. Julien, F. Kober, E. Grillon, J. Derouard, M. Décorps, *C. R. Acad. Sci.* **2000**, *323*, 529 – 536.

[108] X. Zhou, Y. Sun, M. Mazzanti, N. Henninger, J. Mansour, M. Fisher, M. Albert, *NMR Biomed.* **2011**, *24*, 170 – 175.

[109] M. Mazzanti, R. Walvick, X. Zhou, Y. Sun, N. Shah, J. Mansour, J. Gereige, M. Albert, *PLoS One* **2011**, *6*, e21607.

[110] S. S. Kety, *Pharmacol. Rev.* **1951**, *3*, 1 – 41.

[111] C. Landon, P. Berthault, F. Vovelle, H. Desvaux, *Protein Sci.* **2001**, *10*, 762 – 770.

[112] S. M. Rubin, S.-Y. Lee, E. J. Ruiz, A. Pines, D. E. Wemmer, *J. Mol. Biol.* **2002**, *322*, 425 – 440.

[113] A. Bifone, Y. Song, R. Seydoux, R. Taylor, B. Goodson, T. Pietrass, T. Budinger, G. Navon, A. Pines, *Proc. Natl. Acad. Sci. USA* **1996**, *93*, 12932 – 12936.

[114] a) S. C. Gunawardana, D. W. Piston, *Diabetes* **2012**, *61*, 674 – 682; b) X. Liu, S. Wang, Y. You, M. Meng, Z. Zheng, M. Dong, J. Lin, Q. Zhao, C. Zhang, X. Yuan, *Endocrinology* **2015**, *156*, 2461 – 2469.

[115] A. M. Cypess, C. R. Haft, M. R. Laughlin, H. H. Hu, *Cell Metab.* **2014**, *20*, 408 – 415.

[116] P. Thurlby, P. Trayhurn, *Pflügers Arch.* **1980**, *385*, 193 – 201.

[117] R. Branca, L. Zhang, A. Burant, L. Katz, A. McCallister, *Proceedings of the 24th Annual Meeting ISMRM* (Singapore) **2016**, p. 1054.

[118] B. P. Schoenborn, H. C. Watson, J. C. Kendrew, *Nature* **1965**, *207*, 28 – 30.

[119] C. Bowers, V. Storhaug, C. E. Webster, J. Bharatam, A. Cottone, R. Gianna, K. Betsey, B. Gaffney, *J. Am. Chem. Soc.* **1999**, *121*, 9370 – 9377.

[120] L. Dubois, P. Da Silva, C. Landon, J. G. Huber, M. Ponchet, F. Vovelle, P. Berthault, H. Desvaux, *J. Am. Chem. Soc.* **2004**, *126*, 15738 – 15746.

[121] S. M. Rubin, M. M. Spence, I. E. Dimitrov, E. J. Ruiz, A. Pines, D. E. Wemmer, *J. Am. Chem. Soc.* **2001**, *123*, 8616 – 8617.

[122] T. J. Lowery, M. Doucleff, E. J. Ruiz, S. M. Rubin, A. Pines, D. E. Wemmer, *Protein Sci.* **2005**, *14*, 848 – 855.

[123] T. J. Lowery, S. M. Rubin, E. J. Ruiz, A. Pines, D. E. Wemmer, *Angew. Chem. Int. Ed.* **2004**, *43*, 6320 – 6322; *Angew. Chem.* **2004**, *116*, 6480 – 6482.

[124] Y. Song, B. Goodson, R. Taylor, D. Laws, G. Navon, A. Pines, *Angew. Chem. Int. Ed. Engl.* **1997**, *36*, 2368 – 2370; *Angew. Chem.* **1997**, *109*, 2464 – 2466.

[125] a) M. El Haouaj, M. Luhmer, Y. H. Ko, K. Kim, K. Bartik, *J. Chem. Soc. Perkin Trans. 2* **2001**, 804 – 807; b) G. Huber, F. X. Legrand, V. Lewin, D. Baumann, M. P. Heck, P. Berthault, *ChemPhysChem* **2011**, *12*, 1053 – 1055.

[126] a) K. Bartik, M. Luhmer, J.-P. Dutasta, A. Collet, J. Reisse, *J. Am. Chem. Soc.* **1998**, *120*, 784 – 791; b) M. Luhmer, B. Goodson, Y. Song, D. Laws, L. Kaiser, M. Cyrier, A. Pines, *J. Am. Chem. Soc.* **1999**, *121*, 3502 – 3512.

[127] a) M. M. Spence, S. M. Rubin, I. E. Dimitrov, E. J. Ruiz, D. E. Wemmer, A. Pines, S. Q. Yao, F. Tian, P. G. Schultz, *Proc. Natl. Acad. Sci. USA* **2001**, *98*, 10654 – 10657; b) T. Brotin, A. Lesage, L. Emsley, A. Collet, *J. Am. Chem. Soc.* **2000**, *122*, 1171 – 1174.

[128] T. Brotin, J.-P. Dutasta, *Chem. Rev.* **2009**, *109*, 88 – 130.

[129] a) P. A. Hill, Q. Wei, R. G. Eckenhoff, I. J. Dmochowski, *J. Am. Chem. Soc.* **2007**, *129*, 9262 – 9263; b) P. A. Hill, Q. Wei, T. Troxler, I. J. Dmochowski, *J. Am. Chem. Soc.* **2009**, *131*, 3069 – 3077; c) G. Huber, T. Brotin, L. Dubois, H. Desvaux, J.-P. Dutasta, P. Berthault, *J. Am. Chem. Soc.* **2006**, *128*, 6239 – 6246.

[130] a) D. R. Jacobson, N. S. Khan, R. Collé, R. Fitzgerald, L. Laureano-Pérez, Y. Bai, I. J. Dmochowski, *Proc. Natl. Acad. Sci. USA* **2011**, *108*, 10969 – 10973; b) O. Taratula, P. A. Hill, N. S. Khan, P. J. Carroll, I. J. Dmochowski, *Nat. Commun.* **2010**, *1*, 148.

[131] L. Gao, W. Liu, O.-S. Lee, I. J. Dmochowski, J. G. Saven, *Chem. Sci.* **2015**, *6*, 7238 – 7248.

[132] T. J. Lowery, S. Garcia, L. Chavez, E. J. Ruiz, T. Wu, T. Brotin, J. P. Dutasta, D. S. King, P. G. Schultz, A. Pines, *ChemBioChem* **2006**, *7*, 65 – 73.

[133] a) J. Canceill, L. Lacombe, A. Collet, *J. Chem. Soc. Chem. Commun.* **1987**, 219 – 221; b) R. M. Fairchild, A. I. Joseph, K. T. Holman, H. A. Fogarty, T. Brotin, J.-P. Dutasta, C. Boutin, G. Huber, P. Berthault, *J. Am. Chem. Soc.* **2010**, *132*, 15505 – 15507; c) T. Traoré, G. Clavé, L. Delacour, N. Kotera, P.-Y. Renard, A. Romieu, P. Berthault, C. Boutin, N. Tassali, B. Rousseau, *Chem. Commun.* **2011**, *47*, 9702 – 9704; d) Y. Bai, P. A. Hill, I. J. Dmochowski, *Anal. Chem.* **2012**, *84*, 9935 – 9941; e) E. Dubost, N. Kotera, S. Garcia-Argote, Y. Boulard, E. Léonce, C. Boutin, P. Berthault, C. Dugave, B. Rousseau, *Org. Lett.* **2013**, *15*, 2866 – 2868; f) R. Tyagi, C. Witte, R. Haag, L. Schröder, *Org. Lett.* **2014**, *16*, 4436 – 4439.

[134] C. Hilty, T. J. Lowery, D. E. Wemmer, A. Pines, *Angew. Chem. Int. Ed.* **2006**, *45*, 70 – 73; *Angew. Chem.* **2006**, *118*, 76 – 79.

[135] S. Garcia, L. Chavez, T. J. Lowery, S.-I. Han, D. E. Wemmer, A. Pines, *J. Magn. Reson.* **2007**, *184*, 72 – 77.

[136] N. Kotera, N. Tassali, E. Léonce, C. Boutin, P. Berthault, T. Brotin, J. P. Dutasta, L. Delacour, T. Traoré, D. A. Buisson, *Angew. Chem. Int. Ed.* **2012**, *51*, 4100 – 4103; *Angew. Chem.* **2012**, *124*, 4176 – 4179.

[137] K. Ward, A. Aletras, R. Balaban, *J. Magn. Reson.* **2000**, *143*, 79 – 87.

[138] L. Schröder, T. J. Lowery, C. Hilty, D. E. Wemmer, A. Pines, *Science* **2006**, *314*, 446 – 449.

[139] M. Kunth, J. Dopfert, C. Witte, F. Rossella, L. Schröder, *Angew. Chem. Int. Ed.* **2012**, *51*, 8217 – 8220; *Angew. Chem.* **2012**, *124*, 8341 – 8344.

[140] a) L. Schröder, T. Meldrum, M. Smith, T. J. Lowery, D. E. Wemmer, A. Pines, *Phys. Rev. Lett.* **2008**, *100*, 257603; b) L. Schröder, L. Chavez, T. Meldrum, M. Smith, T. J. Lowery, D. E. Wemmer, A. Pines, *Angew. Chem. Int. Ed.* **2008**, *47*, 4316 – 4320; *Angew. Chem.* **2008**, *120*, 4388 – 4392.

[141] F. Schilling, L. Schröder, K. Palaniappan, S. Zapf, D. Wemmer, A. Pines, *ChemPhysChem* **2010**, *11*, 3529 – 3533.

[142] Q. Wei, G. K. Seward, P. A. Hill, B. Patton, I. E. Dimitrov, N. N. Kuzma, I. J. Dmochowski, *J. Am. Chem. Soc.* **2006**, *128*, 13274 – 13283.

[143] V. Roy, T. Brotin, J. P. Dutasta, M. H. Charles, T. Delair, F. Mallet, G. Huber, H. Desvaux, Y. Boulard, P. Berthault, *ChemPhysChem* **2007**, *8*, 2082 – 2085.
[144] J. M. Chambers, P. A. Hill, J. A. Aaron, Z. Han, D. W. Christianson, N. N. Kuzma, I. J. Dmochowski, *J. Am. Chem. Soc.* **2009**, *131*, 563 – 569.
[145] A. Schlundt, W. Kilian, M. Beyermann, J. Sticht, S. Günther, S. Höpner, K. Falk, O. Roetzschke, L. Mitschang, C. Freund, *Angew. Chem. Int. Ed.* **2009**, *48*, 4142 – 4145; *Angew. Chem.* **2009**, *121*, 4206 – 4209.
[146] Ref. [136].
[147] H. M. Rose, C. Witte, F. Rossella, S. Klippel, C. Freund, L. Schröder, *Proc. Natl. Acad. Sci. USA* **2014**, *111*, 11697 – 11702.
[148] G. K. Seward, Y. Bai, N. S. Khan, I. J. Dmochowski, *Chem. Sci.* **2011**, *2*, 1103 – 1110.
[149] C. Boutin, A. Stopin, F. Lenda, T. Brotin, J.-P. Dutasta, N. Jamin, A. Sanson, Y. Boulard, F. Leteurtre, G. Huber, *Bioorg. Med. Chem.* **2011**, *19*, 4135 – 4143.
[150] K. K. Palaniappan, R. M. Ramirez, V. S. Bajaj, D. E. Wemmer, A. Pines, M. B. Francis, *Angew. Chem. Int. Ed.* **2013**, *52*, 4849 – 4853; *Angew. Chem.* **2013**, *125*, 4949 – 4953.
[151] N. S. Khan, B. A. Riggle, G. K. Seward, Y. Bai, I. J. Dmochowski, *Bioconjugate Chem.* **2015**, *26*, 101 – 109.
[152] C. Witte, V. Martos, H. Rose, S. Reinke, S. Klippel, L. Schröder, C. Hackenberger, *Angew. Chem. Int. Ed.* **2015**, *54*, 2806 – 2810; *Angew. Chem.* **2015**, *127*, 2848 – 2852.
[153] B. A. Riggle, Y. Wang, I. J. Dmochowski, *J. Am. Chem. Soc.* **2015**, *137*, 5542 – 5548.
[154] G. K. Seward, Q. Wei, I. J. Dmochowski, *Bioconjugate Chem.* **2008**, *19*, 2129 – 2135.
[155] a) S. Klippel, J. Dopfert, J. Jayapaul, M. Kunth, F. Rossella, M. Schnurr, C. Witte, C. Freund, L. Schröder, *Angew. Chem. Int. Ed.* **2014**, *53*, 493 – 496; *Angew. Chem.* **2014**, *126*, 503 – 506; b) S. Klippel, C. Freund, L. Schröder, *Nano Lett.* **2014**, *14*, 5721 – 5726; c) F. Rossella, H. Rose, C. Witte, J. Jayapaul, L. Schröder, *ChemPlusChem* **2014**, *79*, 1463 – 1471.
[156] T. Meldrum, L. Schröder, P. Denger, D. Wemmer, A. Pines, *J. Magn. Reson.* **2010**, *205*, 242 – 246.
[157] J. Sloniec, M. Schnurr, C. Witte, U. Resch-Genger, L. Schröder, A. Hennig, *Chem. Eur. J.* **2013**, *19*, 3110 – 3118.
[158] M. Schnurr, C. Witte, L. Schröder, *Phys. Chem. Chem. Phys.* **2013**, *15*, 14178 – 14181.
[159] a) M. Schnurr, C. Witte, L. Schröder, *Biophys. J.* **2014**, *106*, 1301 – 1308; b) M. Schnurr, C. Witte, L. Schröder in *Caged Xenon in Phospholipid Membrane Environments* (Eds.: T. Meersmann, E. Brunner), **2015**, Chap. 16, pp. 288 – 300.
[160] K. Jeong, C. C. Slack, C. C. Vassiliou, P. Dao, M. D. Gomes, D. J. Kennedy, A. E. Truxal, L. J. Sperling, M. B. Francis, D. E. Wemmer, *ChemPhysChem* **2015**, *16*, 3573 – 3577.
[161] F. Zamberlan, C. Lesbats, N. J. Rogers, J. L. Krupa, G. E. Pavlovskaya, N. R. Thomas, H. M. Faas, T. Meersmann, *ChemPhysChem* **2015**, *16*, 2294 – 2298.
[162] a) Y. Wang, I. J. Dmochowski, *Chem. Commun.* **2015**, *51*, 8982 – 8985; b) M. Kunth, C. Witte, A. Hennig, L. Schröder, *Chem. Sci.* **2015**, *6*, 6069 – 6075.
[163] M. Schnurr, J. Sloniec-Myszk, J. Döpfert, L. Schröder, A. Hennig, *Angew. Chem. Int. Ed.* **2015**, *54*, 13444 – 13447; *Angew. Chem.* **2015**, *127*, 13645 – 13648.
[164] Y. Wang, B. W. Roose, E. J. Palovcak, V. Carnevale, I. J. Dmochowski, *Angew. Chem. Int. Ed.* **2016**, *55*, 8984 – 8987; *Angew. Chem.* **2016**, *128*, 9130 – 9133.
[165] J. A. Finbloom, C. C. Slack, C. J. Bruns, K. Jeong, D. E. Wemmer, A. Pines, M. B. Francis, *Chem. Commun.* **2016**, *52*, 3119 – 3122.
[166] T. K. Stevens, K. K. Palaniappan, R. M. Ramirez, M. B. Francis, D. E. Wemmer, A. Pines, *Magn. Reson. Med.* **2013**, *69*, 1245 – 1252.
[167] T. Meldrum, K. L. Seim, V. S. Bajaj, K. K. Palaniappan, W. Wu, M. B. Francis, D. E. Wemmer, A. Pines, *J. Am. Chem. Soc.* **2010**, *132*, 5936 – 5937.
[168] M. Schnurr, K. Sydow, H. Rose, M. Dathe, L. Schröder, *Adv. Healthcare Mater.* **2015**, *4*, 40 – 45.
[169] T. K. Stevens, R. M. Ramirez, A. Pines, *J. Am. Chem. Soc.* **2013**, *135*, 9576 – 9579.
[170] M. Shapiro, R. Ramirez, L. Sperling, G. Sun, J. Sun, A. Pines, D. Schaffer, V. Bajaj, *Nat. Chem.* **2014**, *6*, 629 – 634.
[171] Y. Bai, Y. Wang, M. Goulian, A. Driks, I. J. Dmochowski, *Chem. Sci.* **2014**, *5*, 3197 – 3203.
[172] C. Witte, M. Kunth, F. Rossella, L. Schröder, *J. Chem. Phys.* **2014**, *140*, 084203.
[173] M. Zaiss, M. Schnurr, P. Bachert, *J. Chem. Phys.* **2012**, *136*, 144106.
[174] M. Kunth, C. Witte, L. Schröder, *J. Chem. Phys.* **2014**, *141*, 194202.
[175] M. Kunth, C. Witte, L. Schröder, *NMR Biomed.* **2015**, *28*, 601 – 606.
[176] J. Döpfert, C. Witte, M. Kunth, L. Schröder, *Contrast Media Mol. Imaging* **2014**, *9*, 100 – 107.
[177] a) J. Döpfert, C. Witte, L. Schröder, *ChemPhysChem* **2014**, *15*, 261 – 264; b) C. Boutin, E. Léonce, T. Brotin, A. Jerschow, P. Berthault, *J. Phys. Chem. Lett.* **2013**, *4*, 4172 – 4176.
[178] a) A. Y. Louie, M. M. Hüber, E. T. Ahrens, U. Rothbächer, R. Moats, R. E. Jacobs, S. E. Fraser, T. J. Meade, *Nat. Biotechnol.* **2000**, *18*, 321 – 325; b) R. Weissleder, A. Moore, U. Mahmood, R. Bhorade, H. Benveniste, E. A. Chiocca, J. P. Basilion, *Nat. Med.* **2000**, *6*, 351 – 354; c) B. B. Bartelle, C. A. Berríos-Otero, J. J. Rodriguez, A. E. Friedland, O. Aristizábal, D. H. Turnbull, *Circ. Res.* **2012**, *110*, 938 – 947; d) P. S. Patrick, J. Hammersley, L. Loizou, M. I. Kettunen, T. B. Rodrigues, D.-E. Hu, S.-S. Tee, R. Hesketh, S. K. Lyons, D. Soloviev, *Proc. Natl. Acad. Sci. USA* **2014**, *111*, 415 – 420; e) G. G. Westmeyer, Y. Emer, J. Lintelmann, A. Jasanoff, *Chem. Biol.* **2014**, *21*, 422 – 429.
[179] a) G. Genove, U. DeMarco, H. Xu, W. F. Goins, E. T. Ahrens, *Nat. Med.* **2005**, *11*, 450 – 454; b) B. Cohen, H. Dafni, G. Meir, A. Harmelin, M. Neeman, *Neoplasia* **2005**, *7*, 109 – 117.
[180] O. Zurkiya, A. W. S. Chan, X. Hu, *Magn. Reson. Med.* **2008**, *59*, 1225 – 1231.
[181] B. B. Bartelle, M. D. Mana, G. A. Suero-Abreu, J. J. Rodriguez, D. H. Turnbull, *Magn. Reson. Med.* **2015**, *74*, 1750 – 1757.
[182] R. Weissleder, M. Simonova, A. Bogdanova, S. Bredow, W. S. Enochs, J. A. Bogdanov, *Radiology* **1997**, *204*, 425 – 429.
[183] M. G. Shapiro, G. G. Westmeyer, P. A. Romero, J. O. Szablowski, B. Kuster, A. Shah, C. R. Otey, R. Langer, F. H. Arnold, A. Jasanoff, *Nat. Biotechnol.* **2010**, *28*, 264 – U120.
[184] A. A. Gilad, M. T. McMahon, P. Walczak, P. T. Winnard, V. Raman, H. W. van Laarhoven, C. M. Skoglund, J. W. Bulte, P. C. van Zijl, *Nat. Biotechnol.* **2007**, *25*, 217 – 219.
[185] A. Bar-Shir, G. Liu, K. W. Chan, N. Oskolkov, X. Song, N. N. Yadav, P. Walczak, M. T. McMahon, P. C. van Zijl, J. W. Bulte, *ACS Chem. Biol.* **2014**, *9*, 134 – 138.
[186] A. Mukherjee, D. Wu, H. C. Davis, M. G. Shapiro, *bioRxiv* **2016**, 037515.
[187] a) V. D. Kodibagkar, J. Yu, L. Liu, H. P. Hetherington, R. P. Mason, *Magn. Reson. Imaging* **2006**, *24*, 959 – 962; b) L. Liu, V. D. Kodibagkar, J.-X. Yu, R. P. Mason, *FASEB J.* **2007**, *21*, 2014 – 2019; c) Y. Jamin, C. Gabellieri, L. Smyth, S. Reynolds, S. P. Robinson, C. J. Springer, M. O. Leach, G. S. Payne, T. R. Eykyn, *Magn. Reson. Med.* **2009**, *62*, 1300 – 1304.
[188] a) A. P. Chen, R. E. Hurd, Y.-p. Gu, D. M. Wilson, C. H. Cunningham, *NMR Biomed.* **2011**, *24*, 514 – 520; b) P. S. Patrick, M. I. Kettunen, S.-S. Tee, T. B. Rodrigues, E. Serrao, K. N. Timm, S. McGuire, K. M. Brindle, *Magn. Reson. Med.* **2015**, *73*, 1401 – 1406.
[189] a) A. P. Koretsky, B. A. Traxler, *FEBS Lett.* **1989**, *243*, 8 – 12; b) A. P. Koretsky, M. J. Brosnan, L. H. Chen, J. D. Chen, T. Van Dyke, *Proc. Natl. Acad. Sci. USA* **1990**, *87*, 3112 – 3116; c) G. Walter, E. R. Barton, H. L. Sweeney, *Proc. Natl. Acad. Sci. USA* **2000**, *97*, 5151 – 5155.
[190] a) A. K. Srivastava, D. K. Kadayakkara, A. Bar-Shir, A. A. Gilad, M. T. McMahon, J. W. Bulte, *Dis. Models Mech.* **2015**, *8*, 323 – 336; b) A. A. Gilad, K. Ziv, M. T. McMahon, P. C. Van Zijl, M. Neeman, J. W. Bulte, *J. Nucl. Med.* **2008**, *49*, 1905 – 1908; c) A. Jasanoff, *Curr. Opin. Neurobiol.* **2007**, *17*, 593 – 600.
[191] T. Prangé, M. Schiltz, L. Pernot, N. Colloc'h, S. Longhi, W. Bourguet, R. Fourme, *Proteins Struct. Funct. Bioinf.* **1998**, *30*, 61 – 73.
[192] a) E. Locci, Y. Dehouck, M. Casu, G. Saba, A. Lai, M. Luhmer, J. Reisse, K. Bartik, *J. Magn. Reson.* **2001**, *150*, 167 – 174; b) A. Cherubini, A. Bifone, *Prog. Nucl. Magn. Reson. Spectrosc.* **2003**, *42*, 1 – 30.
[193] R. Tilton, Jr., I. Kuntz, Jr., *Biochemistry* **1982**, *21*, 6850 – 6857.
[194] a) F. Pfeifer, *Nat. Rev. Microbiol.* **2012**, *10*, 705 – 715; b) A. Walsby, *Microbiol. Rev.* **1994**, *58*, 94 – 144.
[195] a) E. Harel, L. Schröder, S. Xu, *Annu. Rev. Anal. Chem.* **2008**, *1*, 133 – 163; b) P. van Zijl, N. N. Yadav, *Magn. Reson. Med.* **2011**, *65*, 927 – 948.
[196] M. G. Shapiro, P. W. Goodwill, A. Neogy, M. Yin, F. S. Foster, D. V. Schaffer, S. M. Conolly, *Nat. Nanotechnol.* **2014**, *9*, 311 – 316.

[197] G. J. Lu, A. Farhadi, J. O. Szablowski, S. R. Barnes, A. Lakshmanan, R. W. Bourdeau, M. G. Shapiro, in preparation.
[198] Y. Wang, B. W. Roose, E. J. Palovcak, V. Carnevale, I. J. Dmochowski, *Angew. Chem. Int. Ed.* **2016**, DOI: 10.1002/anie.201604055; *Angew. Chem.* **2016**, DOI: 10.1002/ange.201604055.
[199] A. Farkas, *Ortho-hydrogen, para-Hydrogen, and Heavy Hydrogen*, Cambridge University Press, Cambridge, **1935**.
[200] a) L. Buljubasich, M. B. Franzoni, K. Munnemann, *Top. Curr. Chem.* **2013**, *338*, 33 – 74; b) R. Green, R. Adams, S. Duckett, R. Mewis, D. Williamson, G. Green, *Prog. Nucl. Magn. Reson. Spectrosc.* **2012**, *67*, 1 – 48.
[201] a) B. Feng, A. Coffey, R. Colon, E. Chekmenev, K. Waddell, *J. Magn. Reson.* **2012**, *214*, 258 – 262; b) J. B. Hövener, S. Bar, J. Leupold, K. Jenne, D. Leibfritz, J. Hennig, S. B. Duckett, D. von Elverfeldt, *NMR Biomed.* **2013**, *26*, 124 – 131; c) S. Kadlecek, V. Vahdat, T. Nakayama, D. Ng, K. Emami, R. Rizi, *NMR Biomed.* **2011**, *24*, 933 – 942.
[202] a) P. F. Seidler, H. E. Bryndza, J. E. Frommer, L. S. Stuhl, R. G. Bergman, *Organometallics* **1983**, *2*, 1701 – 1705; b) S. I. Hommeltoft, D. H. Berry, R. Eisenberg, *J. Am. Chem. Soc.* **1986**, *108*, 5345 – 5347.
[203] M. G. Pravica, D. P. Weitekamp, *Chem. Phys. Lett.* **1988**, *145*, 255 – 258.
[204] C. R. Bowers, *eMagRes* **2007**, DOI: 10.1002/9780470034590.emrstm9780470030489.
[205] M. Levitt, *Spin Dynamics: Basics of Nuclear Magnetic Resonance*, Wiley, Chichester, **2001**.
[206] J. K. Gregory, *Acc. Chem. Res.* **1988**, *21*, 120 – 128.
[207] F. Reineri, S. Aime, R. Gobetto, C. Nervi, *J. Chem. Phys.* **2014**, *140*, 094307.
[208] I. Horiuti, M. Polanyi, *Trans. Faraday Soc.* **1934**, *30*, 1164 – 1172.
[209] A. Eichhorn, A. Koch, J. Bargon, *J. Mol. Catal. A* **2001**, *174*, 293 – 295.
[210] D. M. Lilburn, G. E. Pavlovskaya, T. Meersmann, *J. Magn. Reson.* **2013**, *229*, 173 – 186.
[211] a) R. Zhou, E. Zhao, W. Cheng, L. Neal, H. Zheng, R. Quinones, H. Hagelin-Weaver, C. Bowers, *J. Am. Chem. Soc.* **2015**, *137*, 1938 – 1946; b) A. M. Balu, S. B. Duckett, R. Luque, *Dalton Trans.* **2009**, 5074 – 5076.
[212] K. Kovtunov, V. Zhivonitko, I. Skovpin, D. Barskiy, O. Salnikov, I. Koptyug, *J. Phys. Chem. C* **2013**, *117*, 22887 – 22893.
[213] K. Kovtunov, D. Barskiy, R. Shchepin, A. Coffey, K. Waddell, I. Koptyug, E. Chekmenev, *Anal. Chem.* **2014**, *86*, 6192 – 6196.
[214] V. V. Zhivonitko, K. V. Kovtunov, I. V. Skovpin, D. A. Barskiy, O. G. Salnikov, I. V. Koptyug in *Understanding Organometalic Reaction Mechanisms and Catalysis*, Wiley-VCH, Weinheim (Germany), **2014**.
[215] a) K. Kovtunov, D. Barskiy, A. Coffey, M. Truong, O. Salnikov, A. Khudorozhkov, E. Inozemtseva, I. Prosvirin, V. Bukhtiyarov, K. Waddell, E. Chekmenev, I. Koptyug, *Chem. Eur. J.* **2014**, *20*, 11636 – 11639; b) E. Zhao, H. Zheng, K. Ludden, Y. Xin, H. Hagelin-Weaver, C. Bowers, *ACS Catal.* **2016**, *6*, 974 – 978; c) K. Kovtunov, D. Barskiy, O. Salnikov, D. Burueva, A. Khudorozhkov, A. Bukhtiyarov, I. Prosvirin, E. Gerasimov, V. Bukhtiyarov, I. Koptyug, *ChemCatChem* **2015**, *7*, 2581 – 2584.
[216] D. Barskiy, O. Salnikov, K. Kovtunov, I. Koptyug, *J. Phys. Chem. A* **2015**, *119*, 996 – 1006.
[217] A. Corma, O. Salnikov, D. Barskiy, K. Kovtunov, I. Koptyug, *Chem. Eur. J.* **2015**, *21*, 7012 – 7015.
[218] A. Haase, J. Frahm, D. Matthaei, W. Hanicke, K.-D. Merboldt, *J. Magn. Reson.* **1986**, *67*, 258 – 266.
[219] M. D. Robson, P. D. Gatehouse, M. Bydder, G. M. Bydder, *J. Comput. Assist. Tomogr.* **2003**, *27*, 825 – 846.
[220] K. V. Kovtunov, A. S. Romanov, O. G. Salnikov, D. A. Barskiy, E. Y. Chekmenev, I. V. Koptyug, *Tomography* **2016**, *2*, 49 – 55.
[221] K. Kovtunov, M. Truong, D. Barskiy, O. Salnikov, V. Bukhtiyarov, A. Coffey, K. Waddell, I. Koptyug, E. Chekmenev, *J. Phys. Chem. C* **2014**, *118*, 28234 – 28243.
[222] E. Harel, *Lab Chip* **2009**, *9*, 17 – 23.
[223] A. J. Moulé, M. M. Spence, S.-I. Han, J. A. Seeley, K. L. Pierce, S. Saxena, A. Pines, *Proc. Natl. Acad. Sci. USA* **2003**, *100*, 9122 – 9127.
[224] a) J. A. Seeley, S. I. Han, A. Pines, *J. Magn. Reson.* **2004**, *167*, 282 – 290; b) X. Zhou, D. Graziani, A. Pines, *Proc. Natl. Acad. Sci. USA* **2009**, *106*, 16903 – 16906.
[225] C. Hilty, E. E. McDonnell, J. Granwehr, K. L. Pierce, S.-I. Han, A. Pines, *Proc. Natl. Acad. Sci. USA* **2005**, *102*, 14960 – 14963.
[226] J. Granwehr, E. Harel, S. Han, S. Garcia, A. Pines, P. N. Sen, Y.-Q. Song, *Phys. Rev. Lett.* **2005**, *95*, 075503.
[227] E. Harel, J. Granwehr, J. A. Seeley, A. Pines, *Nat. Mater.* **2006**, *5*, 321 – 327.
[228] V. Telkki, J. Saunavaara, J. Jokisaari, *J. Magn. Reson.* **2010**, *202*, 78 – 84.
[229] V. Telkki, C. Hilty, S. Garcia, E. Harel, A. Pines, *J. Phys. Chem. B* **2007**, *111*, 13929 – 13936.
[230] a) V. Telkki, V. Zhivonitko, S. Ahola, K. Kovtunov, J. Jokisaari, I. Koptyug, *Angew. Chem. Int. Ed.* **2010**, *49*, 8363 – 8366; *Angew. Chem.* **2010**, *122*, 8541 – 8544; b) V. Telkki, V. Zhivonitko, *J. Magn. Reson.* **2011**, *210*, 238 – 245; c) V. Zhivonitko, V. Telkki, I. Koptyug, *Angew. Chem. Int. Ed.* **2012**, *51*, 8054 – 8058; *Angew. Chem.* **2012**, *124*, 8178 – 8182.
[231] a) V. Zhivonitko, V. Telkki, J. Leppaniemi, G. Scotti, S. Franssila, I. Koptyug, *Lab Chip* **2013**, *13*, 1554 – 1561; b) V. Telkki, V. Zhivonitko, A. Selent, G. Scotti, J. Leppaniemi, S. Franssila, I. Koptyug, *Angew. Chem. Int. Ed.* **2014**, *53*, 11289 – 11293; *Angew. Chem.* **2014**, *126*, 11471 – 11475.
[232] M. Levitt, *Annu. Rev. Phys. Chem.* **2012**, *63*, 89 – 105.
[233] V. Zhivonitko, K. Kovtunov, P. Chapovsky, I. Koptyug, *Angew. Chem. Int. Ed.* **2013**, *52*, 13251 – 13255; *Angew. Chem.* **2013**, *125*, 13493 – 13497.
[234] A. Tal, L. Frydman, *Prog. Nucl. Magn. Reson. Spectrosc.* **2010**, *57*, 241 – 292.
[235] S. Ahola, V. Zhivonitko, O. Mankinen, G. Zhang, A. Kantola, H. Chen, C. Hilty, I. Koptyug, V. Telkki, *Nat. Commun.* **2015**, *6*, 8363.
[236] a) S. Ahola, V. Telkki, *ChemPhysChem* **2014**, *15*, 1687 – 1692; b) J. King, V. Lee, S. Ahola, V. Telkki, T. Meldrum, *Angew. Chem. Int. Ed.* **2016**, *55*, 5040 – 5043; *Angew. Chem.* **2016**, *128*, 5124 – 5127.
[237] a) N. N. Kuzma, P. Hakansson, M. Pourfathi, R. K. Ghosh, H. Kara, S. J. Kadlecek, G. Pileio, M. H. Levitt, R. R. Rizi, *J. Magn. Reson.* **2013**, *234*, 90 – 94; b) R. K. Ghosh, N. N. Kuzma, S. J. Kadlecek, R. R. Rizi, *Magn. Reson. Med.* **2016**, *75*, 1822 – 1830.
[238] M. S. Freeman, K. Emami, B. Driehuys, *Phys. Rev. A* **2014**, *90*, 023406.

Manuscript received: August 14, 2016
Final Article published: December 5, 2016